PHILOSOPHICAL TRANSACTIONS OF THE ROYAL SOCIETY A MATHEMATICAL, PHYSICAL & ENGINEERING SCIENCES

Elastic Wave Scattering by a Circular Crack

S. Krenk and H. Schmidt

Phil. Trans. R. Soc. Lond. A 1982 **308**, 167-198
doi: 10.1098/rsta.1982.0158

Phil. Trans. R. Soc. Lond. A **308**, 167–198 (1982) [167]
Printed in Great Britain

ELASTIC WAVE SCATTERING BY A CIRCULAR CRACK

BY S. KRENK AND H. SCHMIDT
Risø National Laboratory, DK-4000 Roskilde, Denmark

(*Communicated by F. Ursell, F.R.S. – Received* 26 *October* 1981)

The scattering of waves by a circular crack in an elastic medium is solved by a direct integral equation method. The solution method is based on expansion of stresses and displacements on the crack surface in terms of trigonometric functions and orthogonal polynomials. The expansion coefficients are related through an infinite matrix, and by contour integration the matrix elements are expressed in terms of finite integrals. The scattered far field is expressed explicitly in terms of simple functions and the displacement expansion coefficients. The system of equations is solved numerically, and extensive results are given both in the form of maps of the scattered far field and as scattering cross sections. Neither the method nor the specific results are restricted by any assumptions of symmetry.

1. INTRODUCTION

The problem of scattering of elastic waves by a circular crack is of considerable importance, for example in geophysics, fracture mechanics and ultrasonic testing, and it is therefore natural that it has received some attention. However, useful explicit results are scarce. The reason for this seems to be the mathematical complications of the problem due, at least in part, to the simultaneous generation of longitudinal and transverse waves.

Three steps appear to be necessary in the solution of the general scattering problem. First the problem must be formulated as a boundary value problem in terms of suitable unknown functions. This is quite simple for problems with axial symmetry reducing readily to scalar form, but for oblique angles of incidence vector boundary conditions must also be treated. In most of the literature this problem has been avoided by severe symmetry restrictions. Thus Robertson (1967), Mal (1968*a*, *b*; 1970) and Sih & Loeber (1968, 1969) all considered axisymmetric problems. The problem of a plane transverse wave with normal incidence was considered by Mal (1968*c*), but this problem also involves considerable symmetry. Recently a general formulation of the boundary value problem in terms of integral equations has been given by Martin (1981), but no attempt at a solution is included.

As an explicit, analytic solution of the problem seems unobtainable, the second step must be the derivation of a suitable numerical method. It is crucial that this method retain principal features such as the singular behaviour of the stresses at the crack front. In the literature this has led to transformation of the original dual integral equations to Fredholm integral equations of the second kind. This is accomplished by a transformation of the unknown functions, and in the traditional approach this step introduces Abel integrals that are inconvenient for computations. In the present approach this step is changed, and the displacement discontinuities across the crack are introduced as the unknown functions. This has two immediate consequences. First it facilitates an *a priori* estimate of the required accuracy, and the results have a direct physical interpretation. Secondly, through suitable expansions it leads to a much simpler discretized form of the problem.

Finally, the effectiveness of the method depends on the readiness with which it allows evaluation of specific characteristics of the scattered field, notably the far field and the stress intensity factors. This aspect favours the present method, as the far field can be expressed in closed form in terms of simple functions and the expansion coefficients, and the stress intensity factors are simply linear combinations of the expansion coefficients.

2. Potential and transform representations

The representation of the cylindrical displacement components $\{u, v, w\}$ in terms of scalar potentials and the subsequent expansion of these as Fourier series with Hankel transform coefficients closely follow the presentation of Schmidt & Krenk (1982) and only an outline is given here.

Let $\{r, \theta, z\}$ be a cylindrical coordinate system. The corresponding displacements $\{u, v, z\}$ can then be expressed in terms of three scalar potential functions Φ, Λ and Ψ as

$$u = \frac{\partial \Phi}{\partial r} + \frac{1}{r}\frac{\partial \Psi}{\partial \theta} + \frac{\partial^2 \Lambda}{\partial r\, \partial z} \tag{2.1}$$

$$v = \frac{1}{r}\frac{\partial \Phi}{\partial \theta} - \frac{\partial \Psi}{\partial r} + \frac{1}{r}\frac{\partial^2 \Lambda}{\partial \theta\, \partial z}, \tag{2.2}$$

$$w = \frac{\partial \Phi}{\partial z} - \left\{\frac{1}{r}\frac{\partial}{\partial r}\left(r\frac{\partial}{\partial r}\right) + \frac{1}{r^2}\frac{\partial^2}{\partial \theta^2}\right\}\Lambda. \tag{2.3}$$

The potentials satisfy the scalar wave equations

$$\left(\nabla^2 - \frac{1}{c_{\mathrm{L}}^2}\frac{\partial^2}{\partial t^2}\right)\Phi = 0, \quad \left(\nabla^2 - \frac{1}{c_{\mathrm{T}}^2}\frac{\partial^2}{\partial t^2}\right)(\Lambda, \Psi) = 0, \tag{2.4}$$

where c_{L} and c_{T} are the velocities of longitudinal and transverse waves, respectively.

In the following only vibrations with angular frequency ω will be considered, and displacements, stresses and potentials can then be expressed in complex form with the common factor $\mathrm{e}^{\mathrm{i}\omega t}$. This factor will not be included explicitly in the formulae. Appropriate Fourier expansions of the potentials are

$$\Phi(\eta, \theta, \zeta) = \sum_{m=0}^{\infty} \Phi^m(\eta, \zeta) \begin{Bmatrix} \cos m\theta \\ \sin m\theta \end{Bmatrix}, \tag{2.5}$$

$$\Lambda(\eta, \theta, \zeta) = \sum_{m=0}^{\infty} \Lambda^m(\eta, \zeta) \begin{Bmatrix} \cos m\theta \\ \sin m\theta \end{Bmatrix}, \tag{2.6}$$

$$\Psi(\eta, \theta, \zeta) = \sum_{m=0}^{\infty} \Psi^m(\eta, \zeta) \begin{Bmatrix} \sin m\theta \\ -\cos m\theta \end{Bmatrix}, \tag{2.7}$$

where the characteristic length a has been used to define the dimensionless coordinates $\eta = r/a$ and $\zeta = z/a$.

Substitution of the expansions (2.5)–(2.7) into the wave equations (2.4) and use of the Hankel transform lead to the following representation of the coefficients in the half-space $\zeta > 0$:

$$\Phi^m(\eta, \zeta) = a^2 \int_0^{\infty} A^m(s)\, s\, \mathrm{e}^{-\zeta\alpha(s)} J_m(\eta s)\, \mathrm{d}s, \tag{2.8}$$

$$\Lambda^m(\eta, \zeta) = a^3 \int_0^{\infty} B^m(s)\, s\, \mathrm{e}^{-\zeta\beta(s)} J_m(\eta s)\, \mathrm{d}s, \tag{2.9}$$

$$\Psi^m(\eta, \zeta) = a^2 \int_0^{\infty} C^m(s)\, s\, \mathrm{e}^{-\zeta\beta(s)} J_m(\eta s)\, \mathrm{d}s, \tag{2.10}$$

where $J_m(\ )$ is the Bessel function of the first kind of order m, and

$$\alpha(s) = \begin{cases} (s^2 - h^2)^{\frac{1}{2}}, & s > h, \\ \mathrm{i}(h^2 - s^2)^{\frac{1}{2}}, & s < h, \end{cases} \tag{2.11}$$

$$\beta(s) = \begin{cases} (s^2 - k^2)^{\frac{1}{2}}, & s > k, \\ \mathrm{i}(k^2 - s^2)^{\frac{1}{2}}, & s < k, \end{cases} \tag{2.12}$$

with h and k dimensionless wavenumbers of longitudinal and transverse waves, respectively, which are defined in terms of Poisson's ratio ν, the shear modulus μ and the mass density ρ_0 by

$$h^2 = \left(\frac{\omega a}{c_{\mathrm{L}}}\right)^2 = \frac{1}{2}\frac{(1-2\nu)}{(1-\nu)}\frac{\omega^2 a^2 \rho_0}{\mu}, \tag{2.13}$$

$$k^2 = \left(\frac{\omega a}{c_{\mathrm{T}}}\right)^2 = \frac{\omega^2 a^2 \rho_0}{\mu}. \tag{2.14}$$

The three independent solutions (2.8)–(2.10) are equivalent to those obtained by direct integration by Sezawa (1929).

The displacement components $w(\eta, \theta, \zeta)$, $u(\eta, \theta, \zeta)$ and $v(\eta, \theta, \zeta)$ are expanded in terms of $w^m(\eta, \zeta)$, $u^m(\eta, \zeta)$ and $v^m(\eta, \zeta)$ like (2.5)–(2.7), respectively. In the half-space $\zeta > 0$ the coefficients are

$$\frac{w^m(\eta, \zeta)}{a} = \int_0^\infty \{-A^m(s)\, s\alpha(s)\, \mathrm{e}^{-\zeta\alpha(s)} + B^m(s)\, s^2\, \mathrm{e}^{-\zeta\beta(s)}\}\, J_m(\eta s)\, \mathrm{d}s, \tag{2.15}$$

$$\frac{1}{a}\{u^m(\eta, \zeta) \pm v^m(\eta, \zeta)\} = \int_0^\infty \{\mp A^m(s)\, s^2\, \mathrm{e}^{-\zeta\alpha(s)} \pm B^m(s)\, s\beta(s)\, \mathrm{e}^{-\zeta\beta(s)} + C^m(s)\, s^2\, \mathrm{e}^{-\zeta\beta(s)}\}\, J_{m\pm1}(\eta s)\, \mathrm{d}s. \tag{2.16}$$

The combinations of polar vector components in (2.16) correspond to Cartesian components of Fourier order m and are therefore the natural vector equivalent to the scalar equation (2.15) (Krenk 1979).

The boundary conditions involve the stress components σ_{zz}, σ_{rz} and $\sigma_{\theta z}$. When these components are expanded like (2.5)–(2.7), the resulting integral representations for $\zeta > 0$ are

$$\frac{1}{\mu}\sigma^m_{zz}(\eta, \zeta) = \int_0^\infty \{A^m(s)\, (2s^2 - k^2)\, s\, \mathrm{e}^{-\zeta\alpha(s)} - B^m(s)\, 2s^2\beta(s)\, \mathrm{e}^{-\zeta\beta(s)}\}\, J_m(\eta s)\, \mathrm{d}s, \tag{2.17}$$

$$\frac{1}{\mu}\{\sigma^m_{rz}(\eta, \zeta) \pm \sigma^m_{\theta z}(\eta, \zeta)\} = \int_0^\infty \{\pm A^m(s)\, 2s^2\alpha(s)\, \mathrm{e}^{-\zeta\alpha(s)} \mp B^m(s)\, (2s^2 - k^2)\, s\, \mathrm{e}^{-\zeta\beta(s)} - C^m(s)\, s^2\beta(s)\, \mathrm{e}^{-\zeta\beta(s)}\}\, J_{m\pm1}(\eta s)\, \mathrm{d}s. \tag{2.18}$$

3. Integral equations

The symmetric problem

The symmetric problem is characterized by the two homogeneous conditions

$$\sigma_{rz}(\eta, \theta, 0) \equiv \sigma_{\theta z}(\eta, \theta, 0) \equiv 0. \tag{3.1}$$

Substitution of (2.18) yields

$$A^m(s) = \{(s^2 - \tfrac{1}{2}k^2)/s\alpha(s)\}\, B^m(s), \quad m = 0, 1, \ldots, \tag{3.2}$$

and

$$C^m(s) = 0, \quad m = 0, 1, \ldots. \tag{3.3}$$

Inversion of (2.15) now enables evaluation of the transform function $B^m(s)$ in terms of the displacement coefficient $w^m(\eta, 0)$. When a is taken as the radius of the crack, $w^m(\eta, 0) \equiv 0$ for $\eta > 1$, and the interval of integration is finite:

$$B^m(s) = \frac{2s}{ak^2}\int_0^1 w^m(\eta, 0)\, \eta J_m(\eta s)\, \mathrm{d}\eta. \tag{3.4}$$

When this result is substituted into (2.17), there results a relation between the prescribed normal stress and the as yet unknown normal displacement on the crack surface $0 \leqslant \eta < 1$, $\zeta = 0+$:

$$\frac{1}{\mu}\sigma^m_{zz}(\eta, 0) = \frac{4}{ak^2}\int_0^\infty \{(s^2 - \tfrac{1}{2}k^2)^2 - s^2\alpha(s)\,\beta(s)\}\frac{s}{\alpha(s)} J_m(\eta s)\int_0^1 w^m(\xi, 0)\, \xi J_m(\xi s)\, \mathrm{d}\xi\, \mathrm{d}s. \tag{3.5}$$

For $0 \leqslant \eta < 1$ (3.5) provides an integral equation for the determination of $w^m(\xi, 0)$. It follows from the limit

$$\lim_{s/k\to\infty} 4\{(1-\nu)/k^2\}\{(s^2 - \tfrac{1}{2}k^2)^2 - s^2\alpha(s)\,\beta(s)\}/s\alpha(s) = -1 \tag{3.6}$$

that change of the order of integration would lead to a strongly singular kernel in (3.5). The reason is that (3.5) is stated in terms of its limiting form for $\zeta = 0+$, factors that decay exponentially in s thereby being omitted. When the asymptotic behaviour of the integrand is used to determine the behaviour of $w^m(\xi, 0)$ near the end point $\xi = 1$, the integral equation (3.5) can be solved directly without change of the order of integration, as discussed by Krenk (1981, 1982). This method of solution is described in § 4.

The antisymmetric problem

The antisymmetric problem is slightly more complicated, because the non-homogeneous boundary conditions in this case involve vectors. Antisymmetry gives the homogeneous condition

$$\sigma_{zz}(\eta, \theta, 0) \equiv 0 \tag{3.7}$$

and from (2.17) it follows that

$$B^m(s) = \{(s^2 - \tfrac{1}{2}k^2)/s\beta(s)\}\, A^m(s). \tag{3.8}$$

After elimination of $B^m(s)$, inversion of (2.16) gives $A^m(s)$ and $C^m(s)$ in terms of the displacement coefficients $u^m(\eta, 0) \pm v^m(\eta, 0)$:

$$A^m(s) = \frac{s}{ak^2}\left[-\int_0^1 \{u^m(\eta, 0) + v^m(\eta, 0)\}\, \eta J_{m+1}(\eta s)\, \mathrm{d}\eta + \int_0^1 \{u^m(\eta, 0) - v^m(\eta, 0)\}\, \eta\, J_{m-1}(\eta s)\, \mathrm{d}\eta\right], \tag{3.9}$$

$$C^m(s) = \frac{1}{2as}\left[\int_0^1 \{u^m(\eta, 0) + v^m(\eta, 0)\}\, \eta J_{m+1}(\eta s)\, \mathrm{d}\eta + \int_0^1 \{u^m(\eta, 0) - v^m(\eta, 0)\}\, \eta\, J_{m-1}(\eta s)\, \mathrm{d}\eta\right]. \tag{3.10}$$

Substitution of these relations into (2.18) yields an expression for the shear stresses on the plane $\zeta = 0$ in terms of the in-plane displacements of the crack surface $0 \leqslant \eta < 1$, $\zeta = 0+$:

$$\begin{aligned}\frac{1}{\mu}\{\sigma^m_{rz}(\eta, 0) \pm \sigma^m_{\theta z}(\eta, 0)\} = -\frac{1}{2a}\int_0^\infty \Bigg[\Bigg[\Bigg[\beta(s) - \frac{4}{k^2\beta(s)}\{(s^2 - \tfrac{1}{2}k^2)^2 - s^2\alpha(s)\,\beta(s)\}\Bigg] \\ \times \int_0^1 \{u^m(\xi, 0) \pm v^m(\xi, 0)\}\, \xi\, J_{m\pm1}(\xi s)\, \mathrm{d}\xi \\ + \Bigg[\beta(s) + \frac{4}{k^2\beta(s)}\{(s^2 - \tfrac{1}{2}k^2)^2 - s^2\alpha(s)\,\beta(s)\}\Bigg] \\ \times \int_0^1 \{u^m(\xi, 0) \mp v^m(\xi, 0)\}\, \xi\, J_{m\mp1}(\xi s)\, \mathrm{d}\xi\Bigg]\Bigg] s\, J_{m\pm1}(\eta s)\, \mathrm{d}s.\end{aligned} \tag{3.11}$$

Use of the limit (3.6) shows that change of the order of integration in (3.11) would lead to the same type of strong singularity of the kernels in (3.11) as in (3.5). However, the direct method used to solve (3.5) also works for the coupled equations (3.11). Both problems are therefore treated together in the next section.

The limit (3.6) has been used to identify the asymptotic behaviour of the integrands for fixed k and large values of s. Alternatively it can be used to derive the integral equations of the corresponding static problem by considering the limit $k \to 0$. It is easily verified that this limit gives the integral equations of the static problem given by Krenk (1979).

4. Series representation

The numerical solution is based on the observation that in the limit $s/k \to \infty$ the integral equations (3.5) and (3.11) retain their dominant behaviour while permitting an explicit solution in terms of polynomial expansions. In the general case, $k \neq 0$, the same expansions are used, and their orthogonality properties enable a reformulation of the integral equations as infinite systems of algebraic equations. The solution of the integral equations involve two main steps, namely the evaluation of the matrices of the truncated systems of equations and the solution of the equations. Only the derivation of the matrices is given here. A discussion of the general method including the choice of expansions has been given by Krenk (1981, 1982).

The symmetric problem

The integral equation for the symmetric problem is solved by use of the expansions

$$w^m(\eta, 0) = -a \sum_{j=0}^{\infty} W_j^m P_{m+2j+1}^m\{(1-\eta^2)^{\frac{1}{2}}\}/P_{m+2j+1}^{m+1}(0), \quad 0 \leqslant \eta < 1, \tag{4.1}$$

$$\sigma_{zz}^m(\eta, 0) = \mu \sum_{l=0}^{\infty} S_l^m \frac{(2l+1)!}{(2m+2l+1)!} P_{m+2l+1}^{m+1}(0)\, P_{m+2l+1}^m\{(1-\eta^2)^{\frac{1}{2}}\}/(1-\eta^2)^{\frac{1}{2}}, \quad 0 \leqslant \eta < 1, \tag{4.2}$$

where $P_j^m(\ )$ is the Legendre function of the first kind (Erdelyi 1953). The expansion (4.1) is seen to be of the form $\eta^m(1-\eta^2)^{\frac{1}{2}}$ times an arbitrary even polynomial in η, while (4.2) is η^m times an arbitrary even polynomial in η. The normalizing factors in (4.1) are chosen such that each term approaches $W_j^m(1-\eta^2)^{\frac{1}{2}}$ as $\eta \to 1$. The terms in (4.2) are normalized such that $S_j^m = \frac{1}{2}\pi(1-\nu)^{-1} W_j^m$ in the static limit, $k = 0$.

The inner integral in (3.5) is now evaluated by use of the result

$$\int_0^1 \frac{P_{m+2j+1}^m\{(1-\xi^2)^{\frac{1}{2}}\}}{P_{m+2j+1}^{m+1}(0)} J_m(\xi s)\, \mathrm{d}\xi = (-1)^j s^{-1} j_{m+2j+1}(s), \tag{4.3}$$

where $j_m(\ )$ is the spherical Bessel function of the first kind (Abramowitz & Stegun 1965). This result follows by induction from Sonine's first integral (Krenk 1982). Substitution of the expansion (4.1) into (3.5) then gives

$$\frac{1}{\mu}\sigma_{zz}^m(\eta, 0) = \frac{4}{k^2} \sum_{j=0}^{\infty} (-1)\, W_j^m \int_0^{\infty} \{(s^2 - \tfrac{1}{2}k^2)^2 - s^2\alpha(s)\,\beta(s)\}\,\alpha(s)^{-1} J_m(\eta s) j_{m+2j+1}(s)\, \mathrm{d}s. \tag{4.4}$$

The expansion coefficients S_l^m are then determined by use of the orthogonality relation for the Legendre functions (Erdelyi 1953)

$$\int_0^1 P_{m+2j+1}^m\{(1-\eta^2)^{\frac{1}{2}}\} P_{m+2l+1}^m\{(1-\eta^2)^{\frac{1}{2}}\} \frac{\eta\, \mathrm{d}\eta}{(1-\eta^2)^{\frac{1}{2}}} = \begin{cases} 0, & j \neq l, \\ \dfrac{1}{2m+4j+3} \dfrac{(2m+2j+1)!}{(2j+1)!}, & j = l. \end{cases} \tag{4.5}$$

After change of the order of integration the result can be written as

$$S_l^m = (2m+4l+3)\sum_{j=0}^{\infty}(-1)^{j+l}W_j^m A_{jl}^m, \tag{4.6}$$

where A_{jl}^m are elements of a symmetric complex matrix:

$$A_{jl}^m = -\frac{4}{k^2}\int_0^\infty \frac{(s^2-\frac{1}{2}k^2)^2 - s^2\alpha(s)\,\beta(s)}{s\alpha(s)} j_{m+2j+1}(s)\,j_{m+2l+1}(s)\,\mathrm{d}s. \tag{4.7}$$

The integral in (4.7) can be recast into a form that is more suitable for numerical integration. The principle is to extend the integrand into the complex half-plane $\mathrm{Re}\,s \geqslant 0$ and use contour integration. Details of the procedure are given in Appendix A. When the integration variable is changed to $\xi = s/k$, the integration intervals are $[0, 1]$ and $[0, \gamma]$, where γ is a material constant defined by

$$\gamma^2 = h^2/k^2 = \tfrac{1}{2}(1-2\nu)/(1-\nu) < 1. \tag{4.8}$$

The result is expressed in terms of the spherical Hankel function $h_n^{(2)}(\ )$ in the form

$$A_{jl}^m = \int_0^\gamma \left\{4ki\,\frac{(\xi^2-\frac{1}{2})^2}{\xi(\gamma^2-\xi^2)^{\frac{1}{2}}}\,h_{m+2j+1}^{(2)}(k\xi)\,j_{m+2l+1}(k\xi) + \frac{1}{2m+4j+3}\,\frac{\delta_{jl}}{\xi^2(\gamma^2-\xi^2)^{\frac{1}{2}}}\right\}\mathrm{d}\xi$$
$$+\int_0^1 4ki\,\xi(1-\xi^2)^{\frac{1}{2}}\,h_{m+2j+1}^{(2)}(k\xi)\,j_{m+2l+1}(k\xi)\,\mathrm{d}\xi, \quad j \leqslant l. \tag{4.9}$$

The Kronecker delta δ_{jl} is used to introduce a modification of the integrand of the diagonal elements. The integrals are evaluated numerically by Gaussian quadrature with the square-root weight functions included explicitly, and this makes the particular choice of diagonal modification convenient. The elements $A_{jl}^m, j > l$, follow from symmetry, $A_{jl} = A_{lj}$, and for higher values of m use is made of the recurrence relation

$$A_{j,l}^m = A_{j+1,l+1}^{m-2}. \tag{4.10}$$

The antisymmetric problem

For $m = 0$ the two integral equations (3.11) uncouple because $J_{-1}(x) = -J_1(x)$. The uncoupled equations are

$$\frac{1}{\mu}\sigma_{rz}^0(\eta, 0) = \frac{4}{ak^2}\int_0^\infty \{(s^2-\tfrac{1}{2}k^2)^2 - s^2\alpha(s)\,\beta(s)\}\frac{s}{\beta(s)}J_1(\eta s)\int_0^1 u^0(\xi,.0)\,\xi J_1(\xi s)\,\mathrm{d}\xi\,\mathrm{d}s, \tag{4.11}$$

$$\frac{1}{\mu}\sigma_{\theta z}^0(\eta, 0) = -\frac{1}{a}\int_0^\infty \beta(s)\,sJ_1(\eta s)\int_0^1 v^0(\xi, 0)\,\xi J_1(\xi s)\,\mathrm{d}\xi\,\mathrm{d}s. \tag{4.12}$$

These integral equations describe the radial shear and torsion problems, respectively.

Again, suitable expansions for displacements and stresses are determined from the limiting behaviour of the integrands $s/k \to \infty$. The expansions corresponding to (4.1) and (4.2) with $m = 1$ are

$$\begin{Bmatrix} u^0(\eta, 0) \\ v^0(\eta, 0) \end{Bmatrix} = -a\sum_{j=0}^{\infty}\begin{Bmatrix} U_j^r \\ U_j^\theta \end{Bmatrix} P_{2+2j}^1\{(1-\eta^2)^{\frac{1}{2}}\}/P_{2+2j}^2(0), \quad 0 \leqslant \eta < 1, \tag{4.13}$$

$$\begin{Bmatrix} \sigma_{rz}^0(\eta, 0) \\ \sigma_{\theta z}^0(\eta, 0) \end{Bmatrix} = \mu\sum_{l=0}^{\infty}\begin{Bmatrix} T_l^r \\ T_l^\theta \end{Bmatrix}\frac{(2l+1)!}{(2l+3)!}P_{2+2l}^2(0)\,P_{2+2l}^1\{(1-\eta^2)^{\frac{1}{2}}\}/(1-\eta^2)^{\frac{1}{2}}, \quad 0 \leqslant \eta < 1. \tag{4.14}$$

The integral equations (4.11) and (4.12) are reduced to matrix form by substitution of the displacement expansions (4.13) and use of the orthogonality relation (4.5). The result is

$$T_l^r = (5+4l)\sum_{j=0}^{\infty}(-1)^{j+l}\,U_j^r B_{jl}^1, \tag{4.15}$$

$$T_l^\theta = (5+4l)\sum_{j=0}^{\infty}(-1)^{j+1}\,U_j^\theta C_{jl}^1. \tag{4.16}$$

The matrices B_{jl}^1 and C_{jl}^1 turn out to be special cases of the general matrices B_{jl}^n and C_{jl}^n needed to solve the full antisymmetric problem. They are defined as

$$B_{jl}^n = -\frac{4}{k^2}\int_0^\infty \frac{(s^2-\frac{1}{2}k^2)^2 - s^2\alpha(s)\,\beta(s)}{s\beta(s)}\,j_{n+2j+1}(s)\,j_{n+2l+1}(s)\,\mathrm{d}s, \tag{4.17}$$

$$C_{jl}^n = \int_0^\infty \frac{\beta(s)}{s}\,j_{n+2j+1}(s)\,j_{n+2l+1}(s)\,\mathrm{d}s. \tag{4.18}$$

It is seen that B_{jl}^n follows from A_{jl}^n by exchanging the function $\alpha(s)$ in the denominator with $\beta(s)$. The technique of Appendix A reduces these integrals to

$$B_{jl}^n = \int_0^1 \left\{4ki\,\frac{(\xi^2-\frac{1}{2})^2}{\xi(1-\xi^2)^{\frac{1}{2}}}\,h_{n+2j+1}^{(2)}(k\xi)\,j_{n+2l+1}(k\xi) + \frac{1}{2n+4j+3}\,\frac{\delta_{jl}}{\xi^2(1-\xi^2)^{\frac{1}{2}}}\right\}\mathrm{d}\xi$$
$$+\int_0^\gamma 4ki\,\xi(\gamma^2-\xi^2)^{\frac{1}{2}}\,h_{n+2j+1}^{(2)}(k\xi)\,j_{n+2l+1}(k\xi)\,\mathrm{d}\xi, \quad j\leqslant l, \tag{4.19}$$

$$C_{jl}^n = \int_0^1 \left\{ki\,\xi^{-1}(1-\xi^2)^{\frac{1}{2}}\,h_{n+2j+1}^{(2)}(k\xi)\,j_{n+2l+1}(k\xi) + \frac{1}{2n+4j+3}\,\frac{\delta_{jl}}{\xi^2(1-\xi^2)^{\frac{1}{2}}}\right\}\mathrm{d}\xi, \quad j\leqslant l. \tag{4.20}$$

The remaining elements follow from symmetry, $B_{jl}^n = B_{lj}^n$ and $C_{jl}^n = C_{lj}^n$. In addition use is made of the recurrence relations

$$B_{j,l}^n = B_{j+1,l+1}^{n-2}, \quad C_{j,l}^n = C_{j+1,l+1}^{n-2}. \tag{4.21}$$

The procedure for defining the displacement and stress expansions is easily generalized to the coupled integral equations (3.11) for $m \geqslant 1$. The appropriate values of the indices in the displacement expansions follow from the inner integrals, while the indices of the stress expansions follow from the outer integral. Thus the expansions of $u^m(\eta,0) \pm v^m(\eta,0)$ and $\sigma_{rz}^m(\eta,0) \pm \sigma_{\theta z}^m(\eta,0)$ for $m \geqslant 1$ can be obtained from (4.1) and (4.2) by exchanging m with $m \pm 1$, i.e.

$$u^m(\eta,0) \pm v^m(\eta,0) = -a\sum_{j=0}^{\infty} U_j^{m\pm}\,P_{m\pm1+2j+1}^{m\pm1}\{(1-\eta^2)^{\frac{1}{2}}\}/P_{m\pm1+2j+1}^{m\pm1+1}(0), \quad 0\leqslant\eta<1, \tag{4.22}$$

$$\sigma_{rz}^m(\eta,0) \pm \sigma_{\theta z}^m(\eta,0) = \mu\sum_{l=0}^{\infty} T_l^{m\pm}\,\frac{(2l+1)!}{\{2(m\pm1)+2l+1\}!}\,P_{m\pm1+2l+1}^{m\pm1+1}(0)$$
$$\times P_{m\pm1+2l+1}^{m\pm1+1}\{(1-\eta^2)^{\frac{1}{2}}\}/(1-\eta^2)^{\frac{1}{2}}, \quad 0\leqslant\eta<1. \tag{4.23}$$

When these expansions are substituted into (3.11) the integral equations are reduced to matrix equations by use of the orthogonality relation (4.5). The result is conveniently expressed in terms of the matrices B_{jl}^n and C_{jl}^n defined in (4.17) and (4.18). These definitions are written in terms of a common index n appearing in both of the spherical Bessel functions. The first term of the integral equation (3.11) couples $\sigma_{rz}^m \pm \sigma_{\theta z}^m$ with $u^m \pm v^m$, and clearly $n = m \pm 1$. The second term couples $\sigma_{rz}^m \pm \sigma_{\theta z}^m$ with $u^m \mp v^m$ and leads to a product of spherical Bessel functions that is rewritten as

$$j_{m\mp1+2j+1}(s)\,j_{m\pm1+2l+1}(s) = j_{(m\pm1)+2(j\mp1)+1}(s)\,j_{(m\pm1)+2l+1}(s), \tag{4.24}$$

Thus $n = m \pm 1$ in the second term also, but here j must be replaced by $j \mp 1$. This gives the equations for $m \geqslant 1$:

$$T_l^{m\pm}\{2(m\pm 1)+4l+3\}\sum_{j=0}^{\infty}(-1)^{j+l}\tfrac{1}{2}\{U_j^{m\pm}(B_{jl}^{m\pm 1}+C_{jl}^{m\pm 1})-U_j^{m\mp}(B_{j\mp 1,l}^{m\pm 1}-C_{j\mp 1,l}^{m\pm 1})\}. \quad (4.25)$$

In the static limit, $k = 0$, all the matrices A_{jl}^n, B_{jl}^n and C_{jl}^n reduce to diagonal form

$$\lim_{k\to 0} A_{jl}^n = \lim_{k\to 0} B_{jl}^n = \frac{\delta_{jl}}{(2n+4j+3)}\frac{\pi}{2(1-\nu)}, \quad (4.26)$$

$$\lim_{k\to 0} C_{jl}^n = \frac{\delta_{jl}}{(2n+4j+3)}\frac{\pi}{2}. \quad (4.27)$$

The closed-form solution for $k = 0$ was given by Krenk (1979, 1981). The limit is continuous in the expansion coefficients and has been used to check the numerical calculations.

It is of interest to note that the present solution technique, which follows directly from the systems of one-dimensional integral equations (3.5) and (3.11), may also provide the most direct numerical method of solution of the equivalent two-dimsional vector integral equation given by Martin (1981). In that case the spherical Bessel functions in the matrices A_{jl}^n, B_{jl}^n and C_{jl}^n would come through integrations in the angular direction and not as here through complex contour integration.

Stress intensity factors

The integral relations (3.5) and (3.11) are valid in the full plane of the crack and can therefore be used to determine the behaviour of the stresses at the crack front. The equivalence between the limiting behaviour of the integrands for $s \to \infty$ and the static limit $k \to 0$ enables direct use of the results of the static case as given by Krenk (1981).

The stress components σ_{zz}, σ_{rz} and $\sigma_{\theta z}$ exhibit square-root singularities at the crack front, and their magnitude is determined by the stress intensity factors

$$\begin{Bmatrix} k_1(\theta) \\ k_2(\theta) \\ k_3(\theta) \end{Bmatrix} = \lim_{r\to a+}\{2(r-a)\}^{\frac{1}{2}}\begin{Bmatrix} \sigma_{zz}(r,\theta,0) \\ \sigma_{rz}(r,\theta,0) \\ \sigma_{\theta z}(r,\theta,0) \end{Bmatrix}. \quad (4.28)$$

Formulae for the stress intensity factors in terms of the crack-opening expansion coefficients now follow directly from the results of Krenk (1981):

$$k_1(\theta) = \frac{\mu a^{\frac{1}{2}}}{1-\nu}\sum_{m=0}^{\infty}\begin{Bmatrix}\cos(m\theta)\\ \sin(m\theta)\end{Bmatrix}\sum_{j=0}^{\infty} W_j^m, \quad (4.29)$$

$$k_2(\theta) = \frac{\mu a^{\frac{1}{2}}}{1-\nu}\left[\begin{Bmatrix}1\\0\end{Bmatrix}\sum_{j=0}^{\infty} U_j^r + \sum_{m=1}^{\infty}\begin{Bmatrix}\cos(m\theta)\\ \sin(m\theta)\end{Bmatrix}\sum_{j=0}^{\infty}\tfrac{1}{2}(U_j^{m+}+U_j^{m-})\right], \quad (4.30)$$

$$k_3(\theta) = \mu a^{\frac{1}{2}}\left[\begin{Bmatrix}0\\-1\end{Bmatrix}\sum_{j=0}^{\infty} U_j^\theta + \sum_{m=1}^{\infty}\begin{Bmatrix}\sin(m\theta)\\ -\cos(m\theta)\end{Bmatrix}\sum_{j=0}^{\infty}\tfrac{1}{2}(U_j^{m+}-U_j^{m-})\right]. \quad (4.31)$$

The simplicity of these relations is a consequence of the normalization of the crack-opening displacement expansions at the crack front.

5. The scattered far field

Perhaps the most important aspect of the problem under consideration is the diffraction of the incoming wave. By the separation of the full problem into two parts, the undisturbed original wave and the crack with surface loads, the diffraction emerges from superposition of the original

wave and waves emitted from the crack when subjected to surface loads. The solution of the wave emission problem involves the evaluation of the transform functions $A^m(s)$, $B^m(s)$ and $C^m(s)$ and substitution into the relevant integral representations such as (2.15)–(2.18). Finally, the influence of the distance from the crack is extracted explicitly for the far field, leading to expressions for the angular distribution. As in the previous sections it is convenient to analyse the symmetric and the antisymmetric problems separately and postpone their superposition.

The symmetric problem

In the symmetric problem the transform functions follow from (3.2)–(3.4), (4.1) and (4.3) in the form

$$B^m(s) = \frac{sa(s)}{s^2 - \frac{1}{2}k^2} A^m(s) = \frac{2}{k^2} \sum_{j=0}^{\infty} (-1)^j W_j^m j_{m+2j+1}(s), \tag{5.1}$$

$$C^m(s) = 0. \tag{5.2}$$

The displacements are then obtained from (2.15) and (2.16) as

$$\frac{1}{a} w^m(\eta, \zeta) = \sum_{j=0}^{\infty} (-1)^j W_j^m \frac{2}{k^2} \int_0^{\infty} \{ -(s^2 - \tfrac{1}{2}k^2) \, \mathrm{e}^{-\zeta\alpha(s)} + s^2 \, \mathrm{e}^{-\zeta\beta(s)} \} j_{m+2j+1}(s) \, J_m(\eta s) \, \mathrm{d}s, \tag{5.3}$$

$$\frac{1}{a} \{u^m(\eta, \zeta) \pm v^m(\eta, \zeta)\} = \sum_{j=0}^{\infty} (-1)^j W_j^m \frac{2}{k^2} \int_0^{\infty} \left\{ \mp (s^2 - \tfrac{1}{2}k^2) \frac{s}{\alpha(s)} \mathrm{e}^{-\zeta\alpha(s)} \pm s\beta(s) \, \mathrm{e}^{-\zeta\beta(s)} \right\} j_{m+2j+1}(s) \, J_{m\pm1}(\eta s) \, \mathrm{d}s. \tag{5.4}$$

These expressions can be reformulated by the contour integration method of Appendix A. For $\eta > 1$ the last factor is rewritten in terms of Hankel functions by use of

$$2J_n(\eta s) = H_n^{(1)}(\eta s) + H_n^{(2)}(\eta s), \quad n = m, m \pm 1. \tag{5.5}$$

In this case neither quarter circle contributes, and after combination of pairs of integrals the result for $w^m(\eta, \zeta)$ is

$$\begin{aligned} \frac{1}{a} w^m(\eta, \zeta) = \sum_{j=0}^{\infty} (-1)^j W_j^m \frac{2}{k^2} \Big[\Big[& \mathrm{i} \int_0^h (s^2 - \tfrac{1}{2}k^2) \sin\{\zeta(h^2 - s^2)^{\frac{1}{2}}\} \, j_{m+2j+1}(s) \, H_m^{(2)}(\eta s) \, \mathrm{d}s \\ & - \mathrm{i} \int_0^k s^2 \sin\{\zeta(k^2 - s^2)^{\frac{1}{2}}\} \, j_{m+2j+1}(s) \, H_m^{(2)}(\eta s) \, \mathrm{d}s \\ & + \int_0^{\infty} [(q^2 + \tfrac{1}{2}k^2) \sin\{\zeta(q^2 + h^2)^{\frac{1}{2}}\} - q^2 \sin\{\zeta(q^2 + k^2)^{\frac{1}{2}}\}] \, j_{m+2j+1}(\mathrm{i}q) \, H_m^{(1)}(\mathrm{i}\eta q) \, \mathrm{d}q \Big] \Big]. \end{aligned} \tag{5.6}$$

By changing the integration variable in the last integral to ηq it is easily demonstrated that this integral approaches zero faster than η^{-1} as $\eta \to \infty$. Thus it does not contribute to the dominating far field of diverging waves.

A physical interpretation of the first two integrals is obtained by introducing spherical coordinates $\{\rho, \phi, \theta\}$, related to the cylindrical coordinates $\{\eta, \theta, \zeta\}$ by

$$\eta = \rho \sin\phi, \quad \zeta = \rho \cos\phi. \tag{5.7}$$

After introduction of a trigonometric substitution the far-field contribution to $w^m(\eta,\zeta)$ is

$$\frac{1}{a}w^m(\eta,\zeta) \sim \sum_{j=0}^{\infty}(-1)^j W_j^m \Big\{ 2ih\int_0^{\frac{1}{2}\pi}(\gamma^2\sin^2\psi-\tfrac{1}{2})\cos\psi\sin(\rho h\cos\phi\cos\psi) \times H_m^{(2)}(\rho h\sin\phi\sin\psi)\, j_{m+2j+1}(h\sin\psi)\,\mathrm{d}\psi - 2ik\int_0^{\frac{1}{2}\pi}\sin^2\psi\cos\psi\sin(\rho k\cos\phi\cos\psi) \times H_m^{(2)}(\rho k\sin\phi\sin\psi)\, j_{m+2j+1}(k\sin\psi)\,\mathrm{d}\psi\Big\}. \tag{5.8}$$

No matter how large the value of ρ is, there will be a neighbourhood around zero where the argument of the Hankel function is small. Therefore the interval of integration is divided into two parts by a point $\psi = \Delta(\rho)$ with the property that $\Delta(\rho)\to 0$ and $\rho\Delta(\rho)\to\infty$ as $\rho\to\infty$. A suitable choice of the function $\Delta(\rho)$ is $\Delta(\rho)=\rho^{\delta-1}$, $0<\delta<1$. In the interval $0<\psi<\Delta(\rho)$ an upper bound on the integrand follows from the bound $|H_m^{(2)}(z)| < C_1 + C_2 z^{-m-\epsilon}$ where ϵ is a small positive number, and it is easily seen that this interval contributes terms that are small compared with ρ^{-1}. Thus the dominating contribution comes from the interval $\Delta(\rho)\leqslant\psi\leqslant\frac{1}{2}\pi$, where the Hankel function is replaced by its asymptotic form for large argument:

$$H_m^{(2)}(z) \sim (2/\pi z)^{\frac{1}{2}}\,\mathrm{e}^{-\mathrm{i}\{z-\frac{1}{2}(m+\frac{1}{2})\pi\}}. \tag{5.9}$$

The leading term of $w^m(\eta,\zeta)$ then is

$$\frac{1}{a}w^m(\eta,\zeta) \sim \sum_{j=0}^{\infty}(-1)^j W_j^m (2/\pi)^{\frac{1}{2}}\,\mathrm{e}^{\frac{1}{2}\mathrm{i}(m+\frac{1}{2})\pi} \times\Big[h\int_0^{\frac{1}{2}\pi}(\gamma^2\sin^2\psi-\tfrac{1}{2})\frac{\cos\psi}{(\rho h\sin\phi\sin\psi)^{\frac{1}{2}}}\{\mathrm{e}^{\mathrm{i}\rho h\cos(\theta+\psi)}-\mathrm{e}^{-\mathrm{i}\rho h\cos(\phi-\psi)}\}\, j_{m+2j+1}(h\sin\psi)\,\mathrm{d}\psi - k\int_0^{\frac{1}{2}\pi}\frac{\sin^2\psi\cos\psi}{(\rho k\sin\phi\sin\psi)^{\frac{1}{2}}}\{\mathrm{e}^{\mathrm{i}\rho k\cos(\phi+\psi)}-\mathrm{e}^{-\mathrm{i}\rho k\cos(\phi-\psi)}\}\, j_{m+2j+1}(k\sin\psi)\,\mathrm{d}\psi\Big]. \tag{5.10}$$

When combined with the time factor $\mathrm{e}^{\mathrm{i}\omega t}$ the exponentials in (5.10) are recognized as conical waves propagating along the directions determined by the angles $\phi\pm\psi$. The integrals represent superposition of these conical waves. However, at large distances from the crack, spherical waves of the form $\rho^{-1}\mathrm{e}^{-\mathrm{i}h\rho}$ and $\rho^{-1}\mathrm{e}^{-\mathrm{i}k\rho}$ dominate. This is evident from the asymptotic form of the solution of the problem in spherical coordinates, but also follows from (5.10), when it is observed that all conical waves with $\psi\neq\phi$ cancel at large values of ρ owing to interference. The mathematical analysis demonstrating this is given in Appendix B. By taking out $\rho^{-1}\mathrm{e}^{-\mathrm{i}h\rho}$ and $\rho^{-1}\mathrm{e}^{-\mathrm{i}k\rho}$ as factors, the results of Appendix B give

$$\frac{1}{a}w^m(\eta,\zeta) \sim \sum_{j=0}^{\infty}(-1)^j W_j^m\, 2\mathrm{e}^{\frac{1}{2}\mathrm{i}(m+1)\pi}\{-\rho^{-1}\mathrm{e}^{-\mathrm{i}h\rho}(\gamma^2\sin^2\phi-\tfrac{1}{2})\cot\phi\, j_{m+2j+1}(h\sin\phi) + \rho^{-1}\mathrm{e}^{-\mathrm{i}k\rho}\sin\phi\cos\phi\, j_{m+2j+1}(k\sin\phi)\}. \tag{5.11}$$

It is noted that the function $(r/2\pi)^{\frac{1}{2}}\mathrm{e}^{-\frac{1}{4}\mathrm{i}\pi}\exp\{\mathrm{i}2r\sin^2\frac{1}{2}(\psi-\phi)\}$ acts as a δ-function in the limit $r\to\infty$, while the other contributions vanish.

The asymptotic behaviour of the other displacement components, (5.4), is found in the same way. The conical waves propagated along the normal $0<\psi<\frac{1}{2}\pi$ are produced by integration

along the upper part of the cut complex s-plane. The factors $\alpha(s)$ and $\beta(s)$ from (5.4) therefore contribute with the values $\alpha(s+\mathrm{i}0)$ and $\beta(s+\mathrm{i}0)$, and the result follows immediately from (5.11):

$$\frac{1}{a}\{u^m(\eta,\zeta)\pm v^m(\eta,\zeta)\}\sim\mp\sum_{j=0}^{\infty}(-1)^j W_j^m\, 2\mathrm{e}^{\frac{1}{2}\mathrm{i}(m\pm1)\pi}\{\rho^{-1}\mathrm{e}^{-\mathrm{i}h\rho}(\gamma^2\sin^2\phi-\tfrac{1}{2})j_{m+2j+1}(h\sin\phi)$$
$$+\rho^{-1}\mathrm{e}^{-\mathrm{i}k\rho}\cos^2\phi\, j_{m+2j+1}(k\sin\phi)\}. \quad (5.12)$$

It is noted that the right-hand side of (5.12) is independent of the choice of signs, and therefore the angular displacement component $v(\eta,\theta,\zeta)$ vanishes identically. This is a consequence of the fact that the potential $\Psi(\eta,\theta,\zeta)$ vanishes identically in the symmetric problem.

In terms of the spherical components $\{u_\rho, u_\phi, v\}$ the displacement field takes the simple form

$$\frac{u_\rho}{a}\sim\rho^{-1}\mathrm{e}^{-\mathrm{i}h\rho}\,2\frac{\gamma^2\sin^2\phi-\frac{1}{2}}{\sin\phi}\sum_{m=0}^{\infty}\mathrm{i}^{m-1}\begin{Bmatrix}\cos m\theta\\ \sin m\theta\end{Bmatrix}\sum_{j=0}^{\infty}(-1)^j W_j^m j_{m+2j+1}(h\sin\phi), \quad (5.13)$$

$$\frac{u_\phi}{a}\sim\rho^{-1}\mathrm{e}^{-\mathrm{i}k\rho}\,2\cos\phi\sum_{m=0}^{\infty}\mathrm{i}^{m-1}\begin{Bmatrix}\cos m\theta\\ \sin m\theta\end{Bmatrix}\sum_{j=0}^{\infty}(-1)^j W_j^m j_{m+2j+1}(k\sin\phi). \quad (5.14)$$

As is also clear from the physics of the problem, u_ρ corresponds to a longitudinal wave, while u_ϕ corresponds to a transverse wave. It is seen that part of the dependence on the angle ϕ consists of factors that are independent of m. These factors were identified in the special case $m=0$–i.e. normal incidence of longitudinal waves – by Mal (1970), but the relative magnitude of $|u_\rho|$ and $|u_\phi|$ given was different from that given by (5.13) and (5.14) and is believed to be in error.

The antisymmetric problem

The transform functions of the antisymmetric problem are given by (3.8)–(3.10). Upon substitution of the expansions from § 4, they are of the form

$$A^m(s)=\frac{s\beta(s)}{s^2-\frac{1}{2}k^2}B^m(s)=\frac{1}{k^2}\sum_{j=0}^{\infty}(-1)^j\begin{cases}2U_j^r j_{2+2j}(s), & m=0,\\ U_j^{m+}j_{m+2+2j}(s)-U_j^{m-}j_{m+2j}(s), & m>0,\end{cases} \quad (5.15)$$

$$C^m(s)=\frac{1}{2s^2}\sum_{j=0}^{\infty}(-1)^j\begin{cases}2U_j^\theta j_{2+2j}(s), & m=0,\\ U_j^{m+}j_{m+2+2j}(s)+U_j^{m-}j_{m+2j}(s), & m>0.\end{cases} \quad (5.16)$$

The displacement field then follows from substitution into (2.15) and (2.16):

$$\frac{1}{a}w^m(\eta,\zeta)=\begin{cases}\displaystyle\sum_{j=0}^{\infty}(-1)^j\frac{1}{k^2}\int_0^\infty\left\{s\,\alpha(s)\,\mathrm{e}^{-\zeta\alpha(s)}-(s^2-\tfrac{1}{2}k^2)\frac{s}{\beta(s)}\mathrm{e}^{-\zeta\beta(s)}\right\}\\ \qquad\times 2U_j^r j_{2+2j}(s)\,J_0(\eta s)\,\mathrm{d}s, & m=0,\\ \displaystyle\sum_{j=0}^{\infty}(-1)^j\frac{1}{k^2}\int_0^\infty\left\{s\,\alpha(s)\,\mathrm{e}^{-\zeta\alpha(s)}-(s^2-\tfrac{1}{2}k^2)\frac{s}{\beta(s)}\mathrm{e}^{-\zeta\beta(s)}\right\}\\ \qquad\times\{U_j^{m+}j_{m+2+2j}(s)-U_j^{m-}j_{m+2j}(s)\}J_m(\eta s)\,\mathrm{d}s, & m>0,\end{cases} \quad (5.17)$$

$$\{u^m(\eta,\zeta)\pm v^m(\eta,\zeta)\}=\begin{cases}\displaystyle\sum_{j=0}^{\infty}(-1)^j\int_0^\infty\left[\frac{1}{k^2}\{s^2\mathrm{e}^{-\zeta\alpha(s)}-(s^2-\tfrac{1}{2}k^2)\mathrm{e}^{-\zeta\beta(s)}\}2U_j^r\pm\mathrm{e}^{-\zeta\beta(s)}U_j^\theta\right]\\ \qquad\times j_{2+2j}(s)\,J_1(\eta s)\,\mathrm{d}s, & m=0,\\ \displaystyle\sum_{j=0}^{\infty}(-1)^j\int_0^\infty\left[\pm\frac{1}{k^2}\{s^2\mathrm{e}^{-\zeta\alpha(s)}-(s^2-\tfrac{1}{2}k^2)\mathrm{e}^{-\zeta\beta(s)}\}\{U_j^{m+}j_{m+2+2j}(s)-U_j^{m-}j_{m+2j}(s)\}\right.\\ \qquad\left.+\tfrac{1}{2}\mathrm{e}^{-\zeta\beta(s)}\{U_j^{m+}j_{m+2+2j}(s)+U_j^{m-}j_{m+2j}(s)\}\right]J_{m\pm1}(\eta s)\,\mathrm{d}s, & m>0.\end{cases} \quad (5.18)$$

The asymptotic forms of (5.17) and (5.18) in spherical coordinates follow directly from an analysis similar to that for the symmetric problem:

$$\frac{u_\rho}{a} \sim \rho^{-1}\,\mathrm{e}^{-\mathrm{i}h\rho}\gamma^2\cos\phi\left[2\sum_{j=0}^{\infty}(-1)^j\,U_j^r\,j_{2+2j}(h\sin\phi)+\sum_{m=1}^{\infty}\mathrm{i}^m\begin{Bmatrix}\cos(m\theta)\\ \sin(m\theta)\end{Bmatrix}\right.$$
$$\left.\times\sum_{j=0}^{\infty}(-1)^j\{U_j^{m+}j_{m+2+2j}(h\sin\phi)-U_j^{m-}j_{m+2j}(h\sin\phi)\}\right], \quad (5.19)$$

$$\frac{u_\phi}{a} \sim \rho^{-1}\,\mathrm{e}^{-\mathrm{i}k\rho}\,\frac{\sin^2\phi-\frac{1}{2}}{\sin\phi}\left[2\sum_{j=0}^{\infty}(-1)^j\,U_j^r\,j_{2+2j}(k\sin\phi)+\sum_{m=0}^{\infty}\mathrm{i}^m\begin{Bmatrix}\cos(m\theta)\\ \sin(m\theta)\end{Bmatrix}\right.$$
$$\left.\times\sum_{j=0}^{\infty}(-1)^j\{U_j^{m+}j_{m+2+j}(k\sin\phi)-U_j^{m-}j_{m+2j}(k\sin\phi)\}\right]. \quad (5.20)$$

$$\frac{v}{a} \sim -\rho^{-1}\,\mathrm{e}^{-\mathrm{i}k\rho}\,\tfrac{1}{2}\cot\phi\left[2\sum_{j=0}^{\infty}(-1)^j\,U_j^\theta\,j_{2+2j}(k\sin\phi)+\sum_{m+1}^{\infty}\mathrm{i}^m\begin{Bmatrix}\sin(m\theta)\\ -\cos(m\theta)\end{Bmatrix}\right.$$
$$\left.\times\sum_{j=0}^{\infty}(-1)^j\{U_j^{m+}j_{m+2+2j}(k\sin\phi)+U_j^{m-}j_{m+2j}(k\sin\phi)\}\right]. \quad (5.21)$$

Again u_ρ corresponds to a longitudinal wave, while u_φ and v correspond to transverse waves. In this case also part of the dependence on ϕ appears as factors that are independent of m. The special case of torsion, i.e. only $U_j^\theta \neq 0$, was treated by Mal (1970), who gave a factor $(\sin\phi)^{-1}$ instead of $\cot\phi$ in (5.21). It is clear from the symmetry conditions that a factor $\cos\phi$ must be present.

6. Scattering cross sections and plane waves

An important parameter is the total power scattered by the crack. In the present formulation this quantity is easily evaluated, because the expansions of stresses and surface displacements constitute biorthogonal systems.

The contribution from the symmetric field is

$$\langle P\rangle = \int_0^{2\pi}\int_0^a \mathrm{Re}\{\overline{\mathrm{i}\omega w(r,\theta)}\,\sigma_{zz}(r,\theta)\}\,r\,\mathrm{d}r\,\mathrm{d}\theta \quad (6.1)$$

where the factor $\frac{1}{2}$ from time averaging has been compensated for by the presence of two crack faces. Upon substitution of (4.1) and (4.2) the dimensionless form becomes

$$\left(\frac{\rho_0}{\mu}\right)^{\frac{1}{2}}\frac{\langle P\rangle}{\mu\pi a^2} = 2k\sum_{j=0}^{\infty}\frac{1}{4j+3}\mathrm{Re}\{(\overline{\mathrm{i}W_j^0})\,S_j^0\}+k\sum_{m=1}^{\infty}\sum_{j=0}^{\infty}\frac{1}{2m+4j+3}\mathrm{Re}\{(\overline{\mathrm{i}W_j^m})\,S_j^m\}. \quad (6.2)$$

The formula (6.2) covers the contribution from either the upper or the lower set of trigonometric functions in (2.5)–(2.7). In the general case contributions from both may be present.

The contribution from the antisymmetric field is, similarly,

$$\left(\frac{\rho_0}{\mu}\right)^{\frac{1}{2}}\frac{\langle P\rangle}{\mu\pi a^2} = 2k\sum_{j=0}^{\infty}\frac{1}{4j+5}\mathrm{Re}\{(\overline{\mathrm{i}U_j^r})\,T_j^r+(\overline{\mathrm{i}U_j^\theta})\,T_j^\theta\}$$
$$+\tfrac{1}{2}k\sum_{m=1}^{\infty}\sum_{j=0}^{\infty}\mathrm{Re}\left\{\frac{1}{2m+4j+1}(\overline{\mathrm{i}U_j^{m-}})\,T_j^{m-}+\frac{1}{2m+4j+5}(\overline{\mathrm{i}U_j^{m+}})\,T_j^{m+}\right\}. \quad (6.3)$$

Apart from a few special cases, notably normal wave incidence, both the symmetric and the antisymmetric parts will contribute to the power.

In the special case of incoming plane waves it is customary to relate the scattered power to the power per unit area normal to the incoming wave. This ratio has the dimension area and is called the scattering cross section. For incoming plane longitudinal and transverse waves with amplitude a the power per unit area is given, respectively, by

$$\left(\frac{\rho_0}{\mu}\right)^{\frac{1}{2}}\frac{\langle P_L\rangle}{\mu}=\frac{1}{2\gamma}k^2,\quad \left(\frac{\rho_0}{\mu}\right)^{\frac{1}{2}}\frac{\langle P_T\rangle}{\mu}=\tfrac{1}{2}k^2. \tag{6.4}$$

The scattering cross section as a fraction of the crack area then follows from normalizing the sum of (6.2) and (6.3) with the appropriate expression from (6.4).

It is interesting to compare this way of evaluating the scattering cross section with an alternative method following from a result of Barratt & Collins (1965). The physical content of this result is that the total field can be considered as a superposition of a plane wave and the scattered field. Interference phenomena affecting the amplitude, and thereby the scattered power, can be evaluated in the far field in the direction of the incoming wave, and knowledge of the far field in this particular direction therefore suffices for the determination of the scattering cross section. Mathematically, the result can be expressed in terms of three formulae: one for a pressure wave, one for a vertically polarized shear wave and one for a horizontally polarized shear wave. In the terminology of this paper the respective scattering cross sections Σ_P, Σ_{SV} and Σ_{SH} are determined by

$$\frac{\Sigma_P}{\pi a^2}=-\frac{4}{h}\operatorname{Im}\left(\lim_{\rho\to\infty}\rho\,e^{ih\rho}u_\rho/a\right), \tag{6.5}$$

$$\frac{\Sigma_{SV}}{\pi a^2}=-\frac{4}{k}\operatorname{Im}\left(\lim_{\rho\to\infty}\rho\,e^{ik\rho}u_\phi/a\right), \tag{6.6}$$

$$\frac{\Sigma_{SH}}{\pi a^2}=-\frac{4}{k}\operatorname{Im}\left(\lim_{\rho\to\infty}\rho\,e^{ik\rho}u_\theta/a\right) \tag{6.7}$$

where the displacements correspond to incoming waves of amplitude a, and the spherical angles ϕ and θ correspond to the direction of propagation of the incoming wave.

It is seen that the expressions (6.5)–(6.7) for the scattering cross sections do not involve the crack surface stress expansion coefficients explicitly. On the other hand the identities implied by the two different methods of evaluation imply that the stress expansion coefficients for plane waves are related to the scattered far-field expansion functions. In the numerical calculations presented in the next section the two different ways of evaluating the scattering cross sections have been used to check the far-field expansions against the crack surface stress expansions.

7. Numerical results

The physical problem to be solved can be considered as a superposition of a plane wave and the scattered field. The total stress vector on the crack surface vanishes identically, and the plane wave therefore defines the crack surface stresses to be used in the scattering problem. It is convenient to treat each of the three types of plane wave separately with use of the Cartesian coordinate system $\{x, y, z\}$ indicated in figure 1, while the scattered fields are described in terms of the spherical coordinates $\{r, \phi, \theta\}$ also shown in figure 1. The scattered P-waves correspond to $u_\rho \neq 0$, scattered SV-waves to $u_\phi \neq 0$ and scattered SH-waves to $v \neq 0$. The direction of the incident plane wave is determined by the angles $\phi = \phi_0$ and $\theta = 0$.

The displacement field of the plane P-wave is

$$\begin{Bmatrix} u_x \\ u_y \\ u_z \end{Bmatrix} = u_0 \begin{Bmatrix} \sin\phi_0 \\ 0 \\ \cos\phi_0 \end{Bmatrix} \exp \mathrm{i}\{\omega t - (h/a)\,(x\sin\phi_0 + z\cos\phi_0)\}, \tag{7.1}$$

where u_0 is the amplitude and the time factor $\mathrm{e}^{\mathrm{i}\omega t}$ has been included for clarity. By use of Hooke's law and a change of sign the crack surface stresses of the scattering problem are found to be

$$\begin{Bmatrix} \sigma_{zz} \\ \sigma_{xz} \\ \sigma_{yz} \end{Bmatrix} = \mathrm{i}\mu h \frac{u_0}{a} \begin{Bmatrix} \gamma^{-2} - 2\sin^2\phi_0 \\ \sin 2\phi_0 \\ 0 \end{Bmatrix} \exp\{-\mathrm{i}h(x/a)\sin\phi_0\}. \tag{7.2}$$

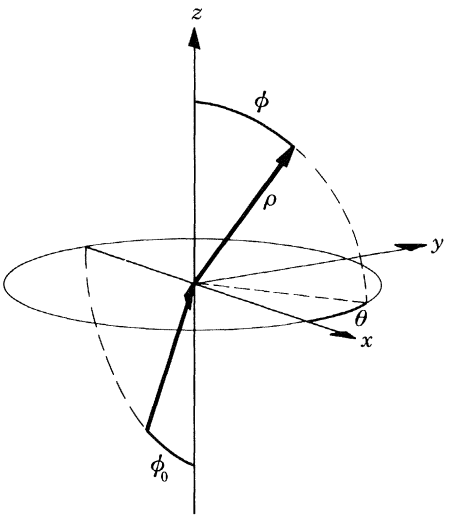

FIGURE 1. Spherical coordinates (ρ, ϕ, θ) and angle of incidence ϕ_0.

The displacement field of the plane SV-wave is

$$\begin{Bmatrix} u_x \\ u_y \\ u_z \end{Bmatrix} = u_0 \begin{Bmatrix} \cos\phi_0 \\ 0 \\ -\sin\phi_0 \end{Bmatrix} \exp \mathrm{i}\{\omega t - (k/a)\,(x\sin\phi_0 + z\cos\phi_0)\} \tag{7.3}$$

and the corresponding crack surface stresses in the scattering problem are

$$\begin{Bmatrix} \sigma_{zz} \\ \sigma_{xz} \\ \sigma_{yz} \end{Bmatrix} = \mathrm{i}\mu k \frac{u_0}{a} \begin{Bmatrix} -\sin 2\phi_0 \\ \cos 2\phi_0 \\ 0 \end{Bmatrix} \exp\{-\mathrm{i}k(x/a)\sin\phi_0\}. \tag{7.4}$$

Finally the displacement field of the plane SH-wave is

$$\begin{Bmatrix} u_x \\ u_y \\ u_z \end{Bmatrix} = u_0 \begin{Bmatrix} 0 \\ 1 \\ 0 \end{Bmatrix} \exp \mathrm{i}\{\omega t - (k/a)\,(x\sin\phi_0 + z\cos\phi_0)\}, \tag{7.5}$$

generating the crack surface stresses

$$\begin{Bmatrix} \sigma_{zz} \\ \sigma_{xz} \\ \sigma_{yz} \end{Bmatrix} = \mathrm{i}\mu k \frac{u_0}{a} \begin{Bmatrix} 0 \\ 0 \\ \cos\phi_0 \end{Bmatrix} \exp\{-\mathrm{i}k(x/a)\sin\phi_0\} \tag{7.6}$$

in the scattering problem.

PHILOSOPHICAL TRANSACTIONS OF THE ROYAL SOCIETY A MATHEMATICAL, PHYSICAL & ENGINEERING SCIENCES

While the crack surface stresses (7.2), (7.4) and (7.6) can be expanded explicitly in the form used in § 4, the general case is more conveniently handled by use of interpolation. In the present case the necessary expansion coefficients were determined by interpolation with $m = 0, \ldots, 7$ and $j = 0, \ldots, 9$.

The scattering cross section, expressed as a fraction of the area of the circle, is given in tables 1–3 for P-, SV- and SH-waves, respectively. It is interesting to observe that for normal incidence, $\phi_0 = 0$, the scattering cross section attains a value close to $2\pi a^2$ for $k \gtrsim 4$. The value is explained

TABLE 1. SCATTERING CROSS SECTIONS FOR INCIDENT P-WAVE

angle of incidence/deg...		0	15	30	45	60	75	90
frequency	Poisson ratio							
0.5	0.05	0.012	0.011	0.008	0.005	0.002	0.001	0.000
	0.15	0.010	0.009	0.007	0.005	0.002	0.001	0.000
	0.25	0.009	0.009	0.007	0.005	0.003	0.001	0.001
	0.35	0.009	0.008	0.007	0.005	0.004	0.003	0.002
	0.45	0.010	0.010	0.009	0.008	0.007	0.007	0.007
1.0	0.05	0.287	0.259	0.188	0.107	0.045	0.011	0.001
	0.15	0.244	0.222	0.167	0.102	0.049	0.017	0.007
	0.25	0.214	0.198	0.156	0.105	0.060	0.032	0.022
	0.35	0.202	0.191	0.161	0.123	0.088	0.064	0.056
	0.45	0.236	0.231	0.215	0.195	0.175	0.161	0.155
2.0	0.05	2.843	2.577	1.913	1.141	0.510	0.129	0.006
	0.15	2.839	2.582	1.937	1.185	0.567	0.191	0.068
	0.25	2.894	2.657	2.059	1.350	0.753	0.381	0.258
	0.35	3.239	3.035	2.509	1.864	1.297	0.929	0.803
	0.45	5.437	5.288	4.889	4.370	3.879	3.536	3.415
3.0	0.05	1.734	1.823	1.790	1.328	0.666	0.176	0.008
	0.15	1.814	1.861	1.779	1.337	0.720	0.252	0.088
	0.25	1.910	1.917	1.801	1.410	0.877	0.456	0.302
	0.35	2.099	2.078	1.952	1.650	1.249	0.920	0.796
	0.45	2.920	2.889	2.792	2.628	2.435	2.278	2.218
4.0	0.05	1.814	1.753	1.577	1.205	0.654	0.183	0.008
	0.15	1.711	1.693	1.569	1.214	0.689	0.247	0.082
	0.25	1.655	1.662	1.581	1.276	0.819	0.431	0.283
	0.35	1.695	1.712	1.676	1.476	1.150	0.859	0.745
	0.45	2.204	2.223	2.249	2.228	2.150	2.062	2.023
5.0	0.05	2.081	1.879	1.493	1.065	0.566	0.157	0.006
	0.15	2.105	1.914	1.519	1.076	0.596	0.208	0.063
	0.25	2.106	1.945	1.577	1.140	0.695	0.349	0.220
	0.35	2.068	1.968	1.704	1.349	0.982	0.702	0.598
	0.45	2.155	2.144	2.100	2.007	1.880	1.769	1.725
6.0	0.05	1.768	1.966	1.832	1.159	0.528	0.137	0.004
	0.15	1.794	1.956	1.841	1.216	0.583	0.184	0.051
	0.25	1.801	1.909	1.818	1.298	0.712	0.323	0.192
	0.35	1.747	1.826	1.812	1.486	1.035	0.698	0.580
	0.45	1.676	1.786	1.992	2.097	2.054	1.956	1.910
7.0	0.05	2.019	1.890	1.652	1.203	0.599	0.155	0.004
	0.15	2.004	1.914	1.696	1.234	0.633	0.196	0.048
	0.25	1.987	1.922	1.733	1.303	0.739	0.327	0.186
	0.35	1.905	1.865	1.745	1.464	1.053	0.712	0.586
	0.45	1.604	1.630	1.686	1.719	1.691	1.633	1.603
8.0	0.05	1.898	1.763	1.445	1.087	0.547	0.136	0.004
	0.15	1.918	1.765	1.465	1.106	0.589	0.180	0.043
	0.25	1.941	1.791	1.500	1.147	0.683	0.301	0.164
	0.35	1.955	1.812	1.542	1.249	0.902	0.608	0.495
	0.45	1.741	1.689	1.586	1.492	1.408	1.337	1.307

by increasing concentration of the scattered field in the form of rays at $\phi = 0$ and 180° for $k \to \infty$. Also, for increasing frequency, the scattered field is increasingly dominated by waves of the same types as the incident wave. The limiting result is a 'shadow' behind the crack and standing waves in front of the crack. This simple conjecture is supported by the scattered fields shown in figures 2 and 7.

Another observation is a seeming resonance phenomenon for P-waves at a frequency around $k \approx 2$. The effect increases with Poisson ratio ν. No similar phenomenon can be observed for

TABLE 2. SCATTERING CROSS SECTIONS FOR INCIDENT SV-WAVE

angle of incidence/deg...		0	15	30	45	60	75	90
frequency	Poisson ratio							
0.5	0.05	0.005	0.006	0.007	0.008	0.007	0.006	0.005
	0.15	0.004	0.005	0.006	0.006	0.006	0.005	0.004
	0.25	0.004	0.004	0.005	0.005	0.005	0.004	0.003
	0.35	0.003	0.003	0.004	0.004	0.004	0.003	0.003
	0.45	0.002	0.003	0.003	0.003	0.003	0.002	0.002
1.0	0.05	0.101	0.123	0.165	0.180	0.150	0.104	0.083
	0.15	0.084	0.101	0.132	0.142	0.120	0.085	0.069
	0.25	0.068	0.081	0.105	0.112	0.095	0.069	0.056
	0.35	0.054	0.064	0.082	0.088	0.075	0.054	0.045
	0.45	0.042	0.048	0.061	0.065	0.055	0.041	0.034
2.0	0.05	1.642	1.649	1.609	1.439	1.172	0.934	0.841
	0.15	1.401	1.442	1.462	1.322	1.051	0.802	0.704
	0.25	1.145	1.220	1.304	1.199	0.928	0.669	0.567
	0.35	0.891	1.010	1.172	1.104	0.825	0.547	0.436
	0.45	0.662	0.865	1.169	1.147	0.812	0.461	0.322
3.0	0.05	2.061	1.860	1.821	2.027	1.841	1.373	1.144
	0.15	2.046	1.801	1.682	1.833	1.624	1.151	0.923
	0.25	1.972	1.700	1.519	1.619	1.403	0.950	0.733
	0.35	1.805	1.538	1.341	1.412	1.200	0.776	0.573
	0.45	1.538	1.305	1.127	1.177	0.983	0.612	0.436
4.0	0.05	2.023	1.788	1.591	1.917	2.043	1.703	1.483
	0.15	2.038	1.748	1.521	1.794	1.816	1.433	1.213
	0.25	2.048	1.690	1.419	1.639	1.571	1.160	0.944
	0.35	2.017	1.602	1.300	1.481	1.338	0.910	0.703
	0.45	1.884	1.460	1.209	1.387	1.167	0.710	0.505
5.0	0.05	2.093	1.866	1.324	1.525	1.825	1.519	1.278
	0.15	2.135	1.834	1.280	1.435	1.616	1.288	1.064
	0.25	2.187	1.779	1.203	1.327	1.405	1.073	0.872
	0.35	2.234	1.696	1.109	1.228	1.212	0.877	0.699
	0.45	2.024	1.565	1.042	1.173	1.047	0.703	0.546
6.0	0.05	1.871	2.046	1.416	1.131	1.583	1.544	1.399
	0.15	1.911	2.044	1.346	1.150	1.561	1.377	1.175
	0.25	1.973	1.975	1.234	1.157	1.494	1.194	0.955
	0.35	2.058	1.800	1.085	1.161	1.402	1.015	0.758
	0.45	2.132	1.602	0.970	1.130	1.299	0.859	0.588
7.0	0.05	1.919	1.902	1.432	1.030	1.451	1.383	1.184
	0.15	1.855	1.961	1.383	1.007	1.334	1.188	0.988
	0.25	1.820	2.012	1.280	0.981	1.207	1.004	0.811
	0.35	1.870	1.980	1.162	0.990	1.108	0.852	0.666
	0.45	1.961	1.751	1.055	1.045	1.037	0.728	0.542
8.0	0.05	2.014	1.755	1.320	0.869	1.150	1.341	1.228
	0.15	2.020	1.798	1.256	0.854	1.163	1.172	1.014
	0.25	1.977	1.872	1.182	0.868	1.128	0.990	0.811
	0.35	1.932	1.926	1.077	0.909	1.068	0.827	0.638
	0.45	1.994	1.810	0.996	0.969	0.996	0.686	0.500

shear waves. There is a general decrease of the scattering cross section with the angle of incidence, although the scattering cross section for SV-waves exhibits a local extremum in the interval $0 < \phi < 90°$.

Figure 2 shows the scattered field from an incident P-wave with $\phi_0 = 0$ at the frequencies $k = 2$, 4 and 8. Owing to axial symmetry the field is completely determined by the sections given in the figure. The SH-waves vanish identically. With increasing frequency the scattered P-waves are concentrated as rays, while the SV-waves degenerate into a more complicated pattern.

TABLE 3. SCATTERING CROSS SECTIONS FOR INCIDENT SH-WAVE

angle of incidence/deg...		0	15	30	45	60	75	90
frequency	Poisson ratio							
0.5	0.05	0.005	0.005	0.004	0.002	0.001	0.000	0.000
	0.15	0.004	0.004	0.003	0.002	0.001	0.000	0.000
	0.25	0.004	0.003	0.003	0.002	0.001	0.000	0.000
	0.35	0.003	0.003	0.002	0.001	0.001	0.000	0.000
	0.45	0.002	0.002	0.002	0.001	0.001	0.000	0.000
1.0	0.05	0.101	0.093	0.072	0.046	0.022	0.006	0.000
	0.15	0.084	0.077	0.060	0.038	0.018	0.005	0.000
	0.25	0.068	0.063	0.049	0.031	0.015	0.004	0.000
	0.35	0.054	0.050	0.039	0.025	0.012	0.003	0.000
	0.45	0.042	0.038	0.030	0.019	0.009	0.002	0.000
2.0	0.05	1.642	1.462	1.033	0.576	0.240	0.056	0.000
	0.15	1.401	1.248	0.883	0.493	0.205	0.048	0.000
	0.25	1.145	1.020	0.723	0.404	0.169	0.040	0.000
	0.35	0.891	0.794	0.564	0.317	0.133	0.031	0.000
	0.45	0.662	0.591	0.421	0.238	0.100	0.024	0.000
3.0	0.05	2.061	1.873	1.379	0.788	0.327	0.075	0.000
	0.15	2.046	1.848	1.340	0.754	0.309	0.071	0.000
	0.25	1.972	1.774	1.275	0.711	0.289	0.066	0.000
	0.35	1.805	1.625	1.169	0.652	0.266	0.060	0.000
	0.45	1.538	1.392	1.016	0.575	0.237	0.054	0.000
4.0	0.05	2.023	2.048	1.787	1.111	0.461	0.102	0.000
	0.15	2.038	2.047	1.763	1.083	0.445	0.098	0.000
	0.25	2.048	2.037	1.725	1.046	0.426	0.094	0.000
	0.35	2.017	1.994	1.670	1.002	0.405	0.089	0.000
	0.45	1.884	1.873	1.581	0.952	0.384	0.084	0.000
5.0	0.05	2.093	1.950	1.674	1.148	0.510	0.115	0.000
	0.15	2.135	1.967	1.664	1.135	0.503	0.113	0.000
	0.25	2.187	1.983	1.642	1.115	0.493	0.111	0.000
	0.35	2.234	1.985	1.599	1.082	0.480	0.108	0.000
	0.45	2.204	1.934	1.532	1.035	0.461	0.104	0.000
6.0	0.05	1.871	1.816	1.501	1.031	0.489	0.115	0.000
	0.15	1.911	1.835	1.498	1.020	0.481	0.113	0.000
	0.25	1.973	1.858	1.491	1.008	0.472	0.110	0.000
	0.35	2.058	1.873	1.468	0.995	0.463	0.107	0.000
	0.45	2.132	1.859	1.417	0.976	0.457	0.105	0.000
7.0	0.05	1.919	1.934	1.347	1.018	0.581	0.144	0.000
	0.15	1.855	1.929	1.349	1.003	0.570	0.141	0.000
	0.25	1.820	1.930	1.344	0.986	0.558	0.138	0.000
	0.35	1.870	1.952	1.328	0.966	0.546	0.134	0.000
	0.35	1.961	1.949	1.294	0.946	0.531	0.129	0.000
8.0	0.05	2.014	1.830	1.302	1.025	0.534	0.121	0.000
	0.15	2.020	1.847	1.304	1.018	0.535	0.122	0.000
	0.25	1.977	1.868	1.304	1.002	0.535	0.123	0.000
	0.35	1.932	1.887	1.291	0.978	0.531	0.123	0.000
	0.45	1.994	1.902	1.259	0.949	0.522	0.122	0.000

PHILOSOPHICAL TRANSACTIONS OF THE ROYAL SOCIETY A MATHEMATICAL, PHYSICAL & ENGINEERING SCIENCES

In problems without axial symmetry more extensive plots are necessary to illustrate the far field. The sections are now supplemented by contours connecting points of equal amplitude on a large spherical shell. Owing to the symmetry of the problem with respect to the xz-plane only one of the intervals $0 \leqslant \theta \leqslant 180°$ and $180 \leqslant \theta \leqslant 360°$ needs consideration. Figures 3–5 illustrate the amplitudes of the scattered far field from an incident P-wave with $\phi_0 = 45°$. The upper semicircles contain contour plots of the spherical shell on the diffraction side, with ϕ and θ as polar coordinates in the intervals $0 \leqslant \phi \leqslant 90°$ and $0 \leqslant \theta \leqslant 180°$, while the lower semicircles show the reflexion side with $180° - \phi$ and θ as polar coordinates in the intervals $90 \leqslant \phi \leqslant 180°$ and $180 \leqslant \theta \leqslant 360°$. Each semicircle can be envisaged as the unfolded quarter of a spherical shell. The magnitudes associated with the contours can be inferred from the corresponding sections shown by solid lines for $\theta = 0, 180°$ and by dotted lines for $\theta = 90, 270°$.

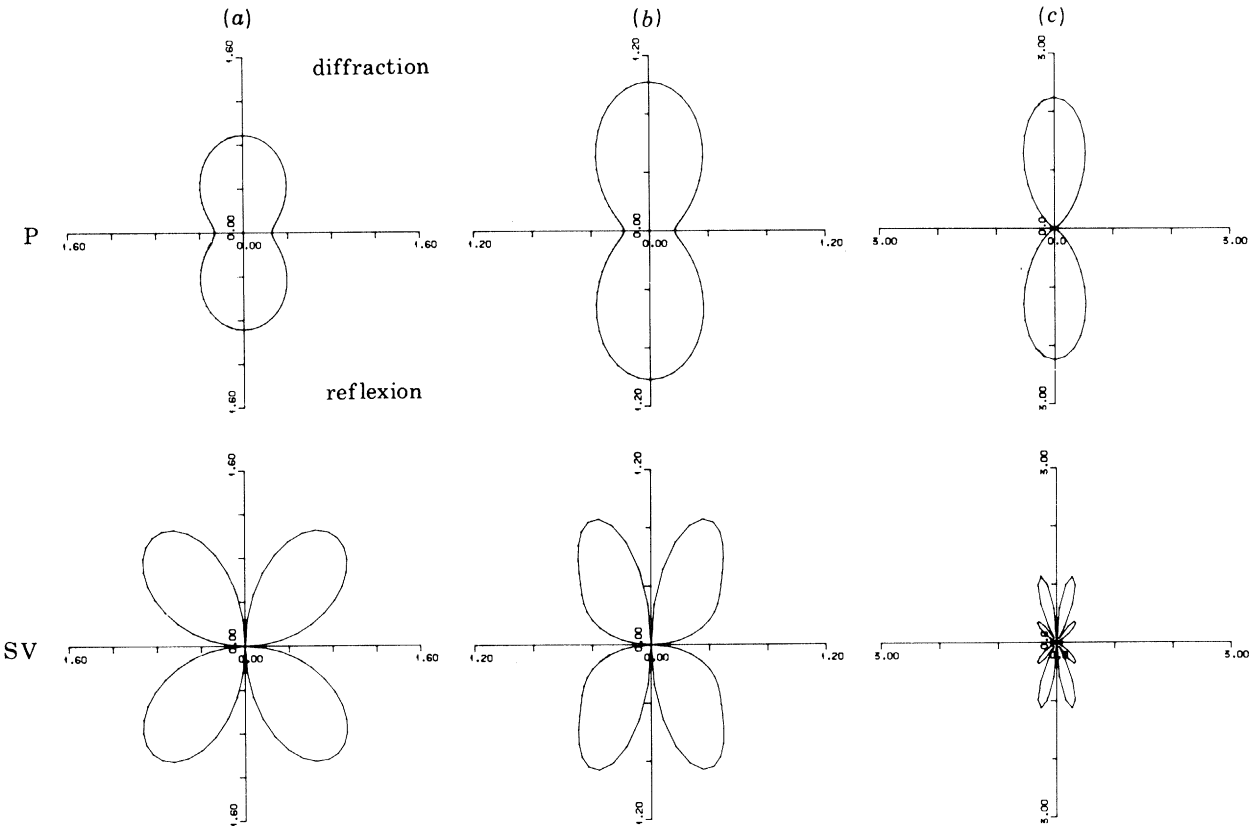

FIGURE 2. Amplitudes of scattered waves from incoming P-wave with $\phi_0 = 0$. Frequencies k are (a) 2, (b) 4, (c) 8.

The problem of the inclined P-wave also contains a scattered SH-component. For $k = 2$ the P- and SV-lobes are tilted slightly, and for $k = 4$ both the diffraction and the reflexion lobes of the P-wave are tilted forward, while the backward SV-lobe degenerates. At $k = 8$ the SH-contribution has diminished and P- and SV-waves have clear ray character. The angle of the reflected SV-wave is predicted quite accurately by the formula for reflexion by a free surface (see for example Achenbach (1973, p. 175):

$$-\sin\phi_{SV} = \gamma \sin\phi_0. \tag{7.7}$$

With $\phi_0 = 45°$ and $\nu = 0.25$ this gives $\phi_{SV} = 156°$.

Figure 6 shows amplitude sections for an incident P-wave parallel to the crack, $\phi_0 = 90°$. The magnitude of the scattered field depends strongly on the Poisson ratio ν as shown in table 1. For low values of k ($k \lesssim 1$) the scattered field approaches that generated by an incident P-wave with $\phi_0 = 0$ but is scaled by the factor $\nu/(1-\nu)$. As k increases the lobes of both P- and SV-waves shift forward, and for $k = 8$ the angles $\phi_{SV} = 36°$ and $\phi_{SV} = 144°$ from (7.7) again accurately predict the behaviour of the scattered SV-waves.

Figure 7 shows the diffraction of a SV-wave with $\phi_0 = 0$. This case also covers the SH-wave with $\phi_0 = 0$. As for an incident P-wave with $\phi_0 = 0$ the scattered waves of the same type as the

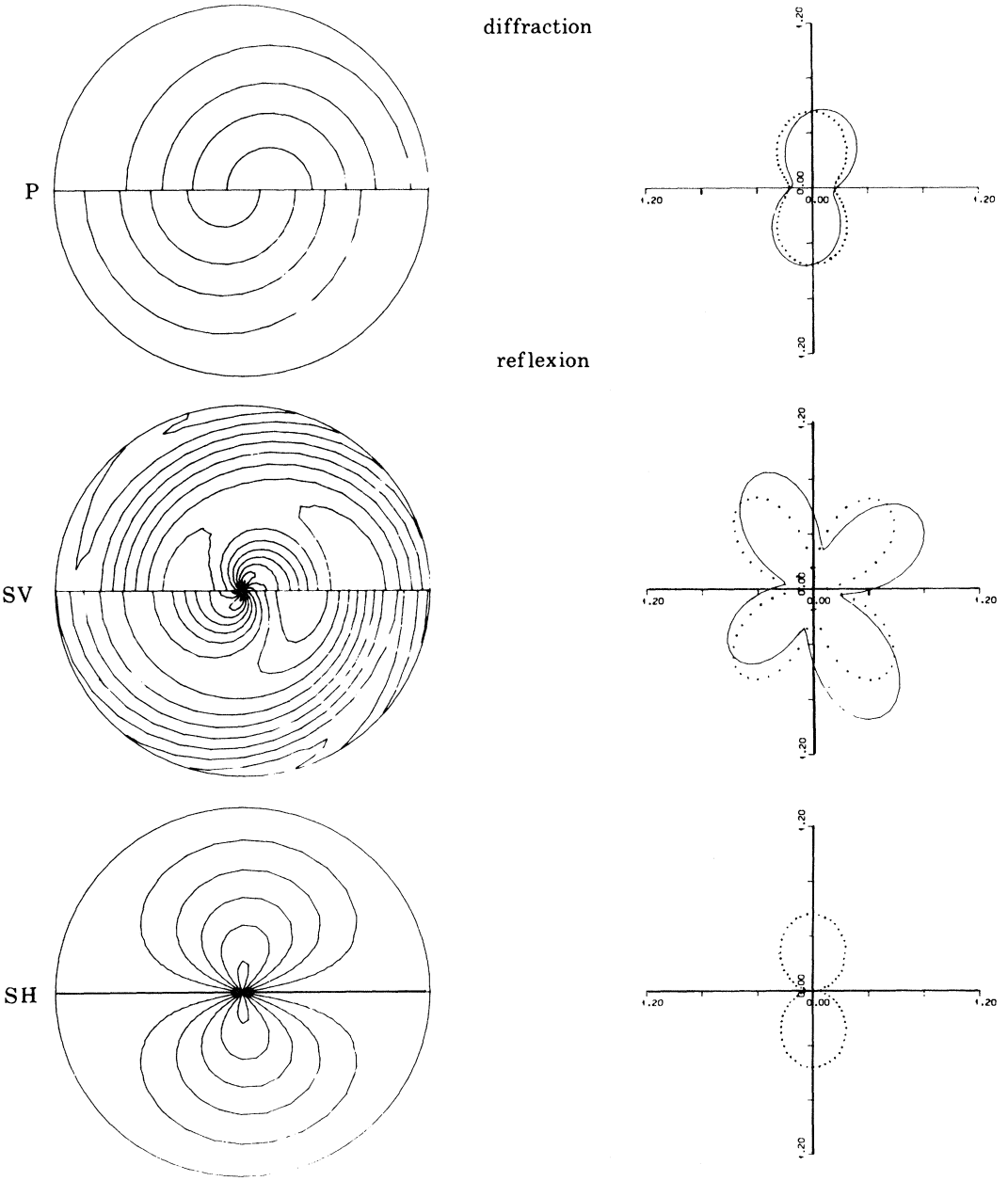

FIGURE 3. Amplitude contours and sections of scattered waves from incoming P-wave with $\phi_0 = 45°$. Frequency $k = 2$.

incident wave approach rays at $\phi_0 = 0$ and 180°, while the waves of different type diminish with increasing frequency.

An incident SV-wave with $\phi_0 = 45°$ only induces normal stresses on the crack surface, and the corresponding scattering problem is similar to that for an incident P-wave with $\phi_0 = 90°$ apart from the different wave length. For $\phi_0 = 90°$ the lobes correspond to those for $\phi_0 = 0$ for small values of k, while for increasing values of k they first shift forward and then transform to a forward ray and a backward ray.

The far field corresponding to an incident SV-wave with $\phi_0 = 30°$ is shown in figures 8–10. At low frequencies the scattered SV-waves follow an approximately doubly symmetric pattern,

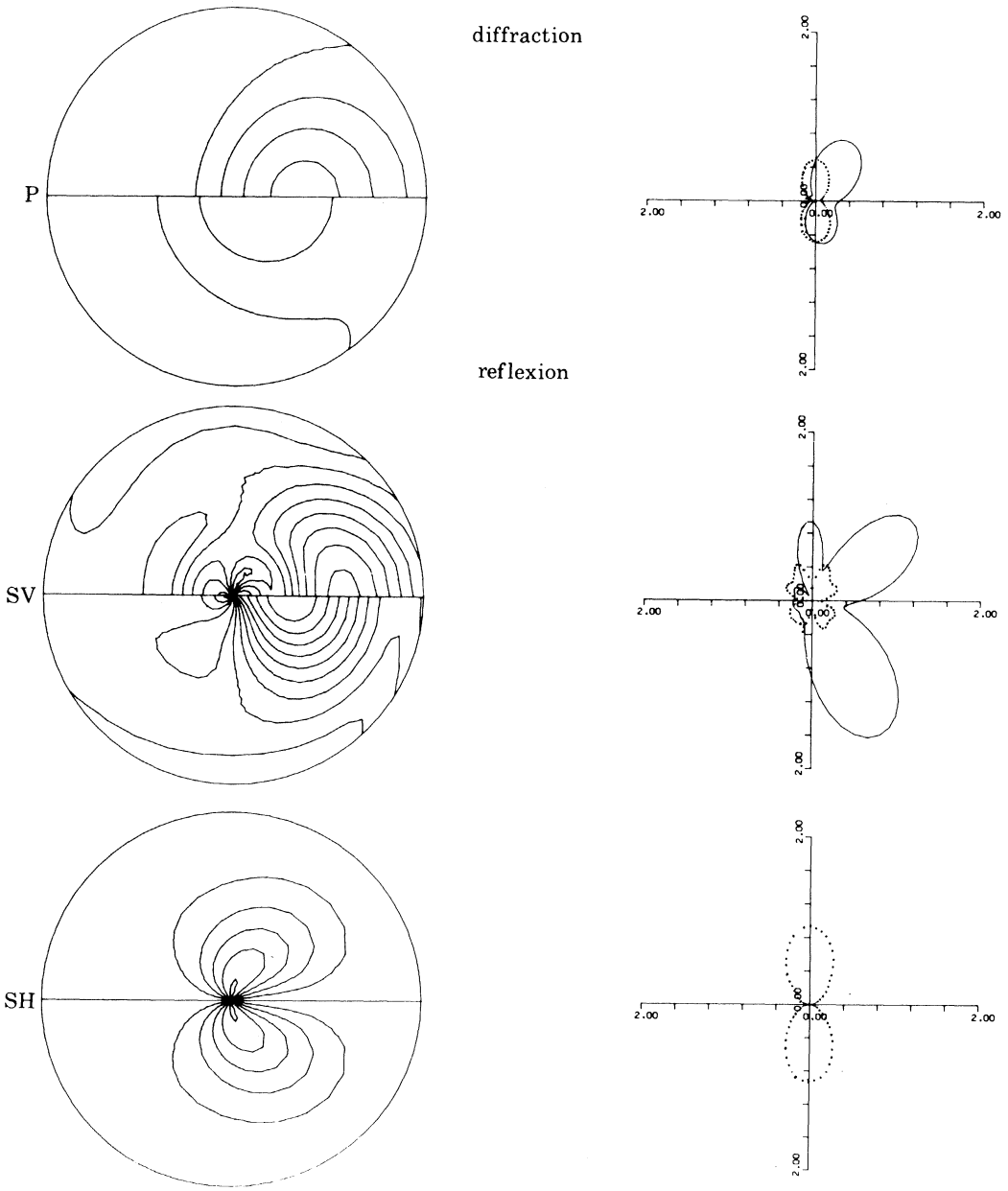

FIGURE 4. Amplitude contours and sections of scattered waves from incoming P-wave with $\phi_0 = 45°$. Frequency $k = 4$.

tilted at 30°. With increasing frequency the scattered SV-waves are concentrated in a ray behind the crack, presumably producing a shadow in the limit $k \to \infty$. The apparent singularity of the contour plots of SV- and SH-waves at $\phi = 0$ and 180° is a consequence of the decomposition in spherical coordinates and does not represent a physical singularity.

The scattering of an incident SH-wave with $\phi_0 = 0$ has already been illustrated by figure 7. The far field corresponding to an incident SH-wave with $\phi_0 = 30°$ is shown in figures 11–13. The scattered SH-waves become increasingly dominating with increasing frequency and develop ray character.

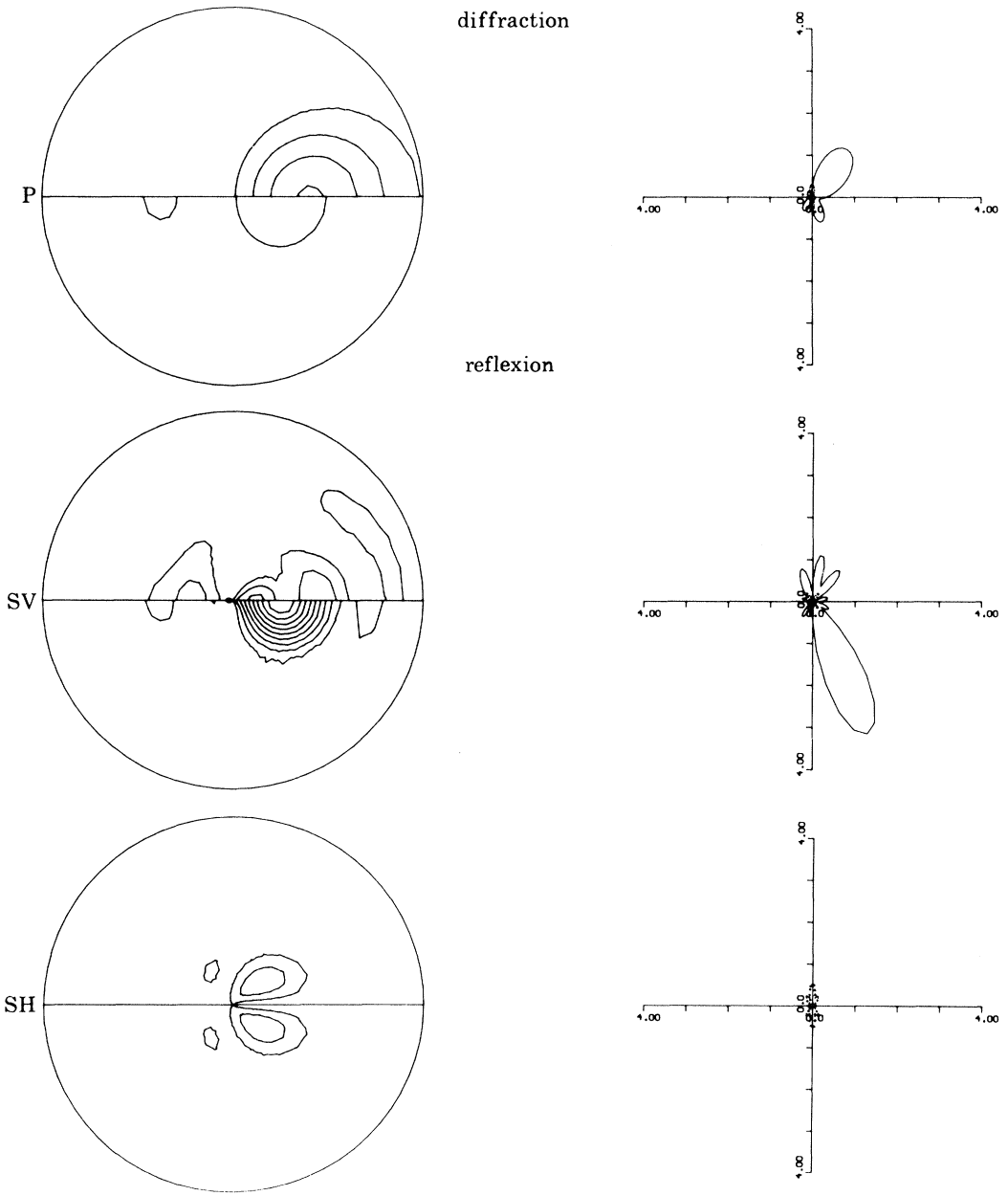

FIGURE 5. Amplitude contours and sections of scattered waves from incoming P-wave with $\phi_0 = 45°$. Frequency $k = 8$.

8. Discussion and conclusions

A formulation of the elastic wave scattering problem for a circular crack has been developed. By use of Hankel transforms the problem is reduced to a system of singular integral equations (3.5) and (3.11) of a type previously investigated by one of the authors. The unknown functions are the Fourier coefficients of the crack-opening displacements and the right-hand sides are the Fourier coefficients of the corresponding crack surface stresses.

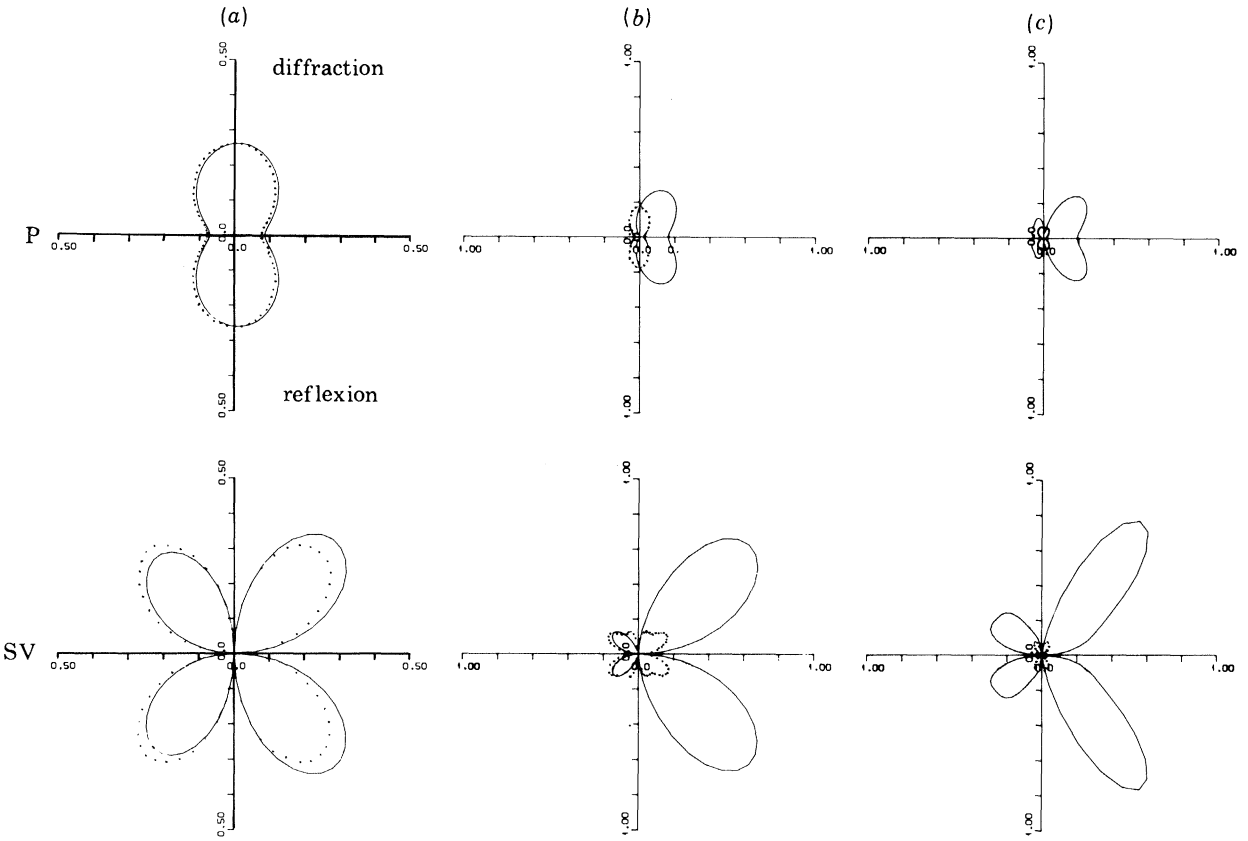

Figure 6. Amplitudes of scattered waves from incoming P-wave with $\phi_0 = 90°$. Frequencies k are (*a*) 2, (*b*) 4 and (*c*) 8.

The integral equations are solved numerically by expanding the Fourier coefficients in terms of associated Legendre functions of integer indices, i.e. a suitable weight function and polynomials. The solution technique provides direct matrix relations (4.6), (4.15), (4.16) and (4.25) between the crack-opening displacement expansion coefficients and the crack surface stress expansion coefficients. These matrices approach diagonal form with decreasing frequency, and the static problem allows a simple explicit solution. Convenient and computationally efficient formulae (4.9), (4.19) and (4.20) are given for the dynamic case.

The stress intensity factors are given as sums of the crack-opening displacement expansion coefficients by (4.29)–(4.31). Even more important are the far-field expansions derived in § 5. They give the scattered far field in spherical coordinates as explicit series in trigonometric functions, spherical Bessel functions and the crack-opening displacement expansion coefficients. In § 6 explicit formulae for the scattering cross section in terms of the crack-opening displacement

expansion coefficients are given. Finally, numerical results for the scattering cross section and the far field are presented and discussed in § 7.

In conclusion, the computational method may be said to consist of three main parts: expansions of stresses and displacements on the crack surface, matrix relations between these two sets of coefficients, and, finally, formulae expressing the near field and the far field explicitly in terms of the coefficients. As the method accounts correctly for the singularity at the crack front, it is highly accurate, and inclusion of the proper singular weight function also leads to very simple explicit expressions for the stress intensity factors as well as the scattered far field.

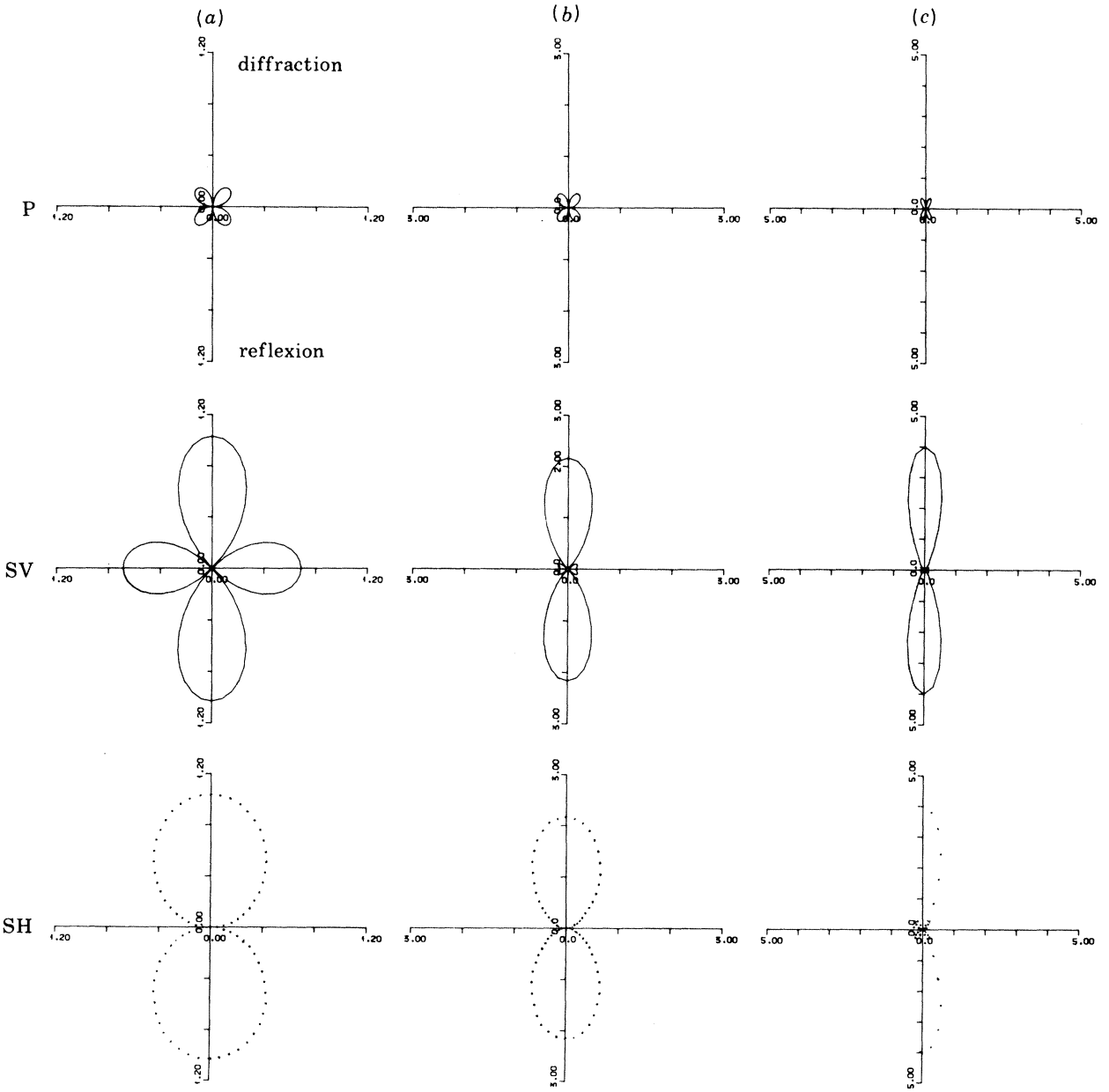

FIGURE 7. Amplitudes of scattered waves from incoming SV-wave with $\phi_0 = 0$. Frequencies k are (*a*) 2, (*b*) 4 and (*c*) 8.

PHILOSOPHICAL TRANSACTIONS OF THE ROYAL SOCIETY A MATHEMATICAL, PHYSICAL & ENGINEERING SCIENCES

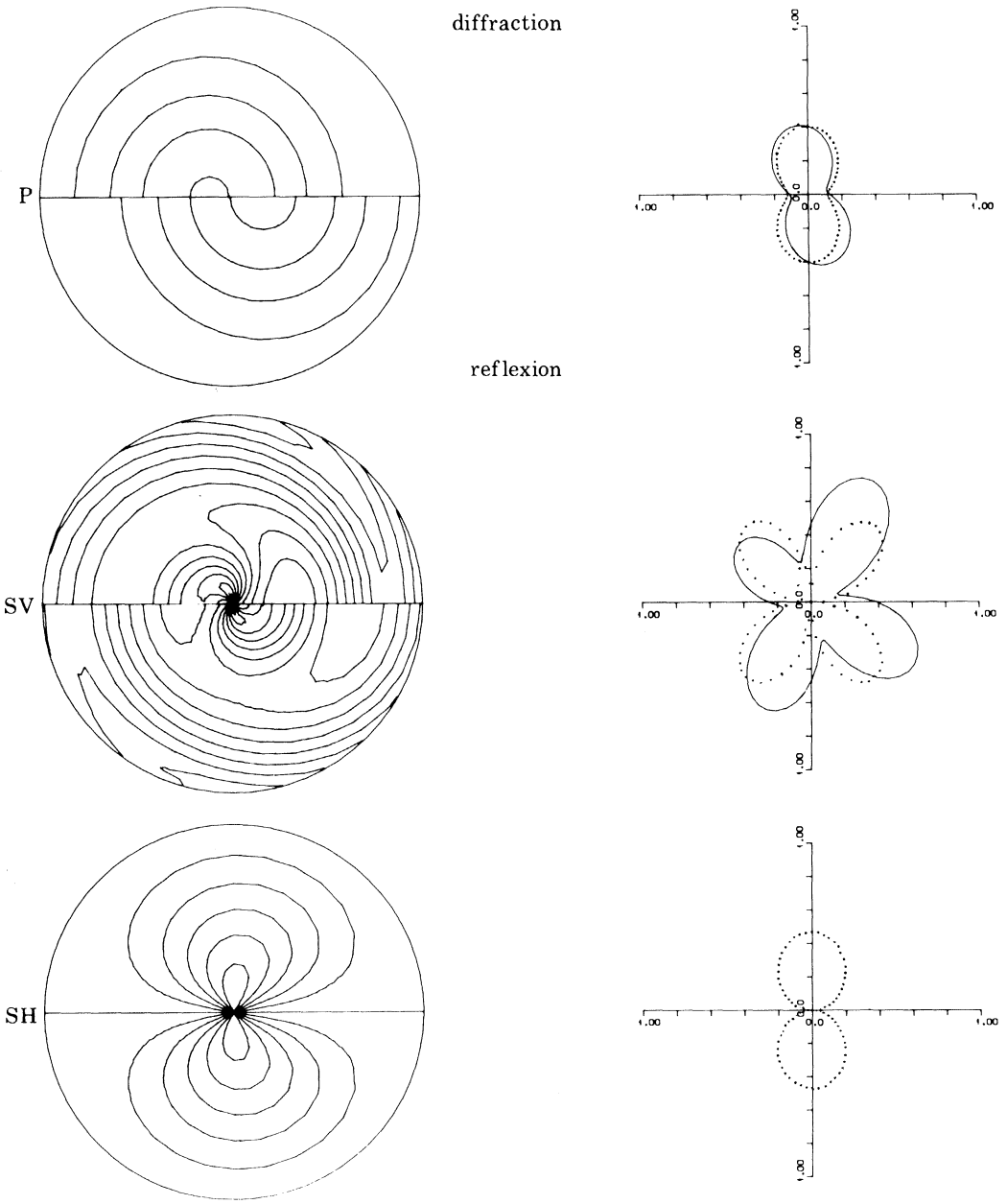

FIGURE 8. Amplitude contours and sections of scattered waves from incoming SV-wave with $\phi_0 = 30°$. Frequency $k = 2$.

PHILOSOPHICAL TRANSACTIONS OF THE ROYAL SOCIETY A MATHEMATICAL, PHYSICAL & ENGINEERING SCIENCES

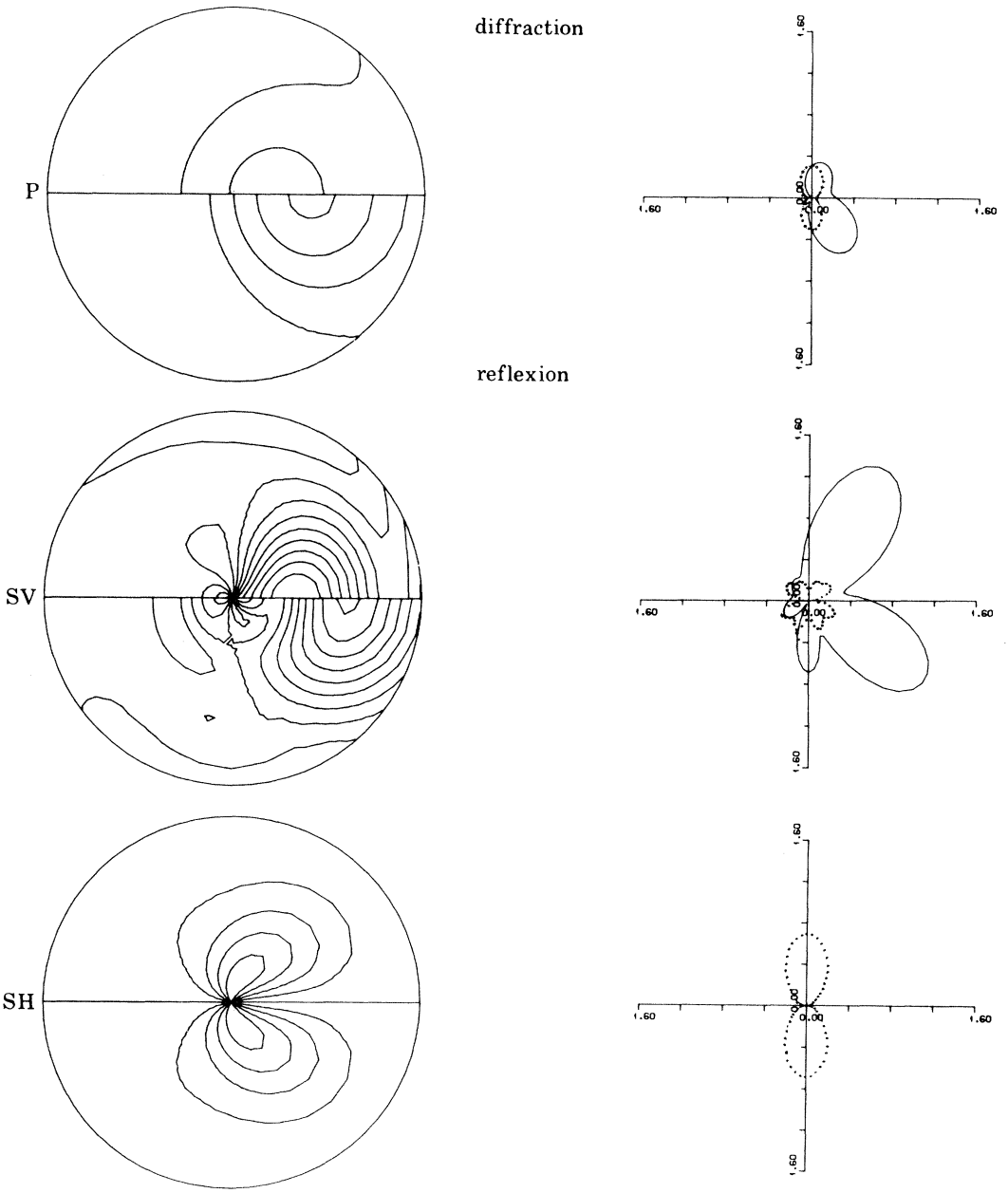

FIGURE 9. Amplitude contours and sections of scattered waves from incoming SV-wave with $\phi_0 = 30°$. Frequency $k = 4$.

PHILOSOPHICAL TRANSACTIONS OF THE ROYAL SOCIETY A MATHEMATICAL, PHYSICAL & ENGINEERING SCIENCES

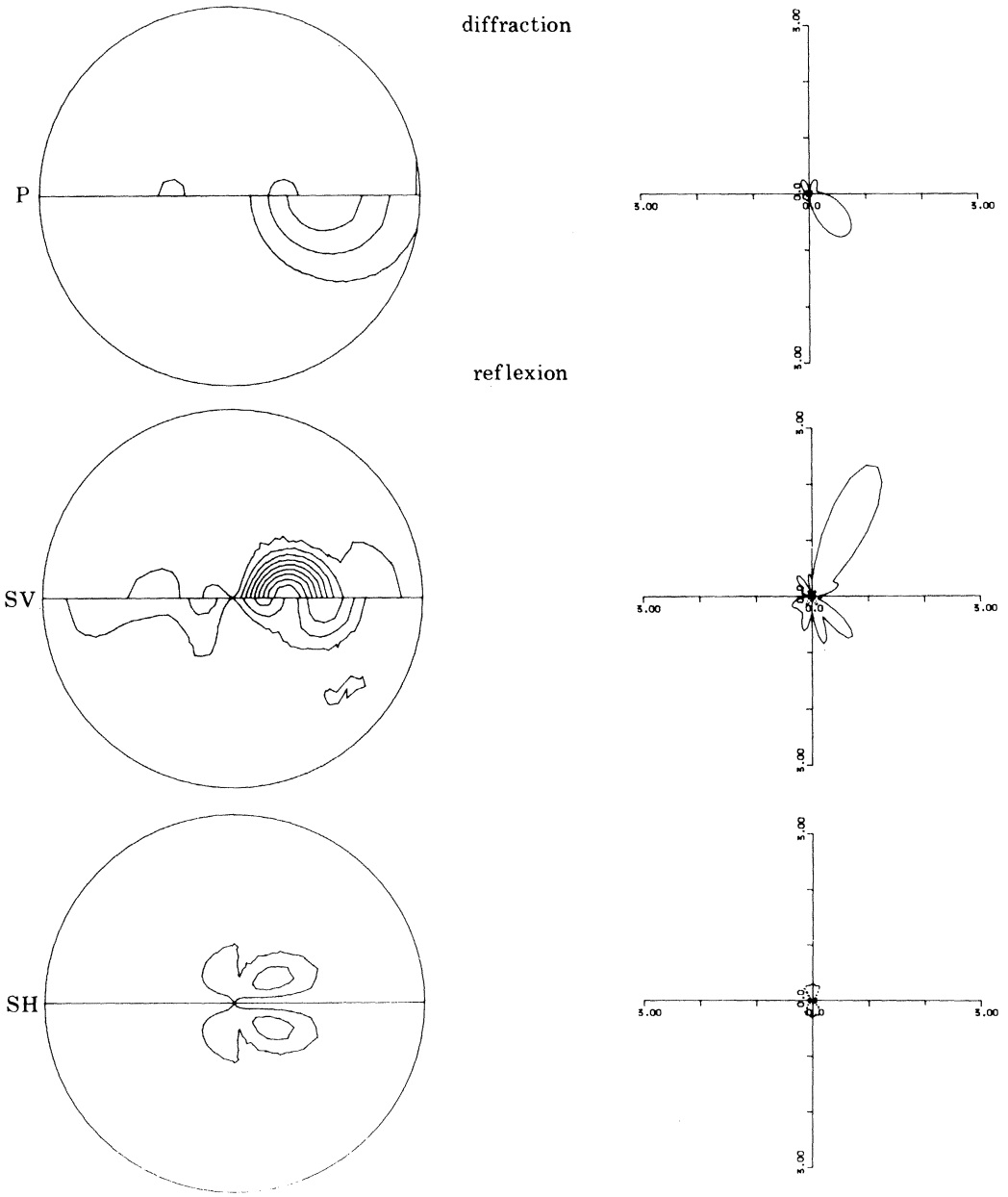

FIGURE 10. Amplitude contours and sections of scattered waves from incoming SV-wave with $\phi_0 = 30°$. Frequency $k = 8$.

PHILOSOPHICAL TRANSACTIONS OF THE ROYAL SOCIETY A MATHEMATICAL, PHYSICAL & ENGINEERING SCIENCES

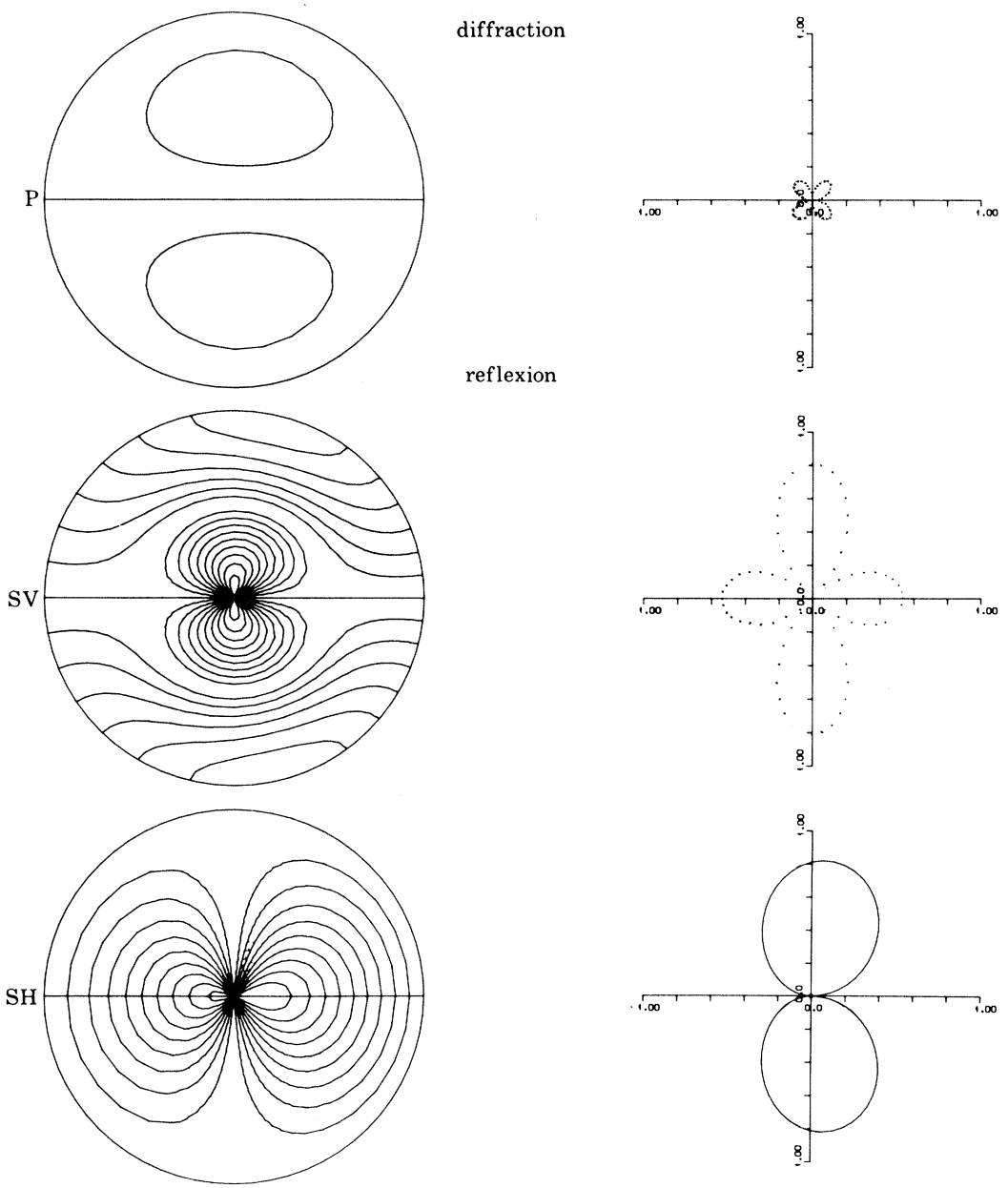

FIGURE 11. Amplitude contours and sections of scattered waves from incoming SH-wave with $\phi_0 = 30°$. Frequency $k = 2$.

PHILOSOPHICAL TRANSACTIONS OF THE ROYAL SOCIETY A MATHEMATICAL, PHYSICAL & ENGINEERING SCIENCES

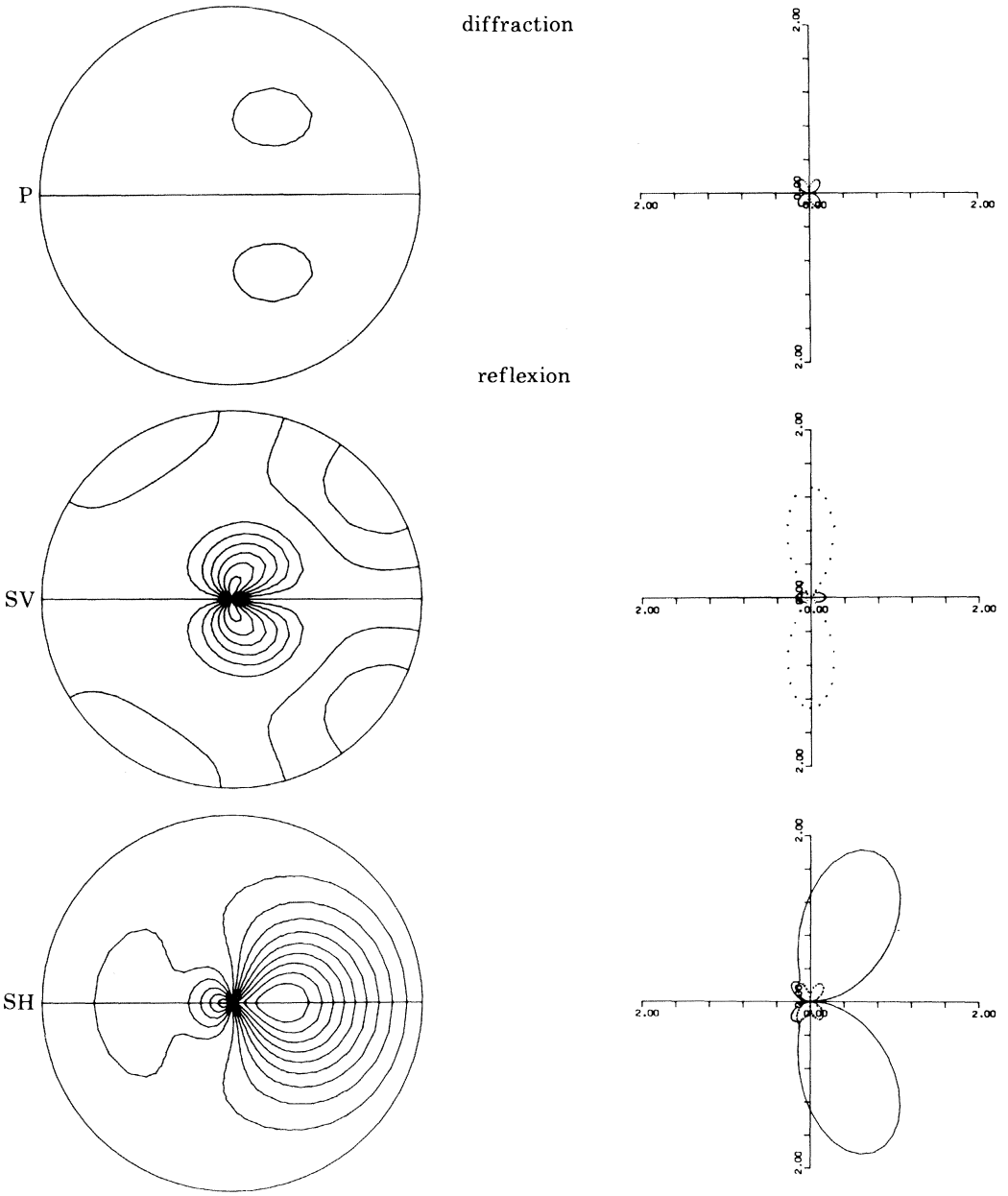

FIGURE 12. Amplitude contours and sections of scattered waves from incoming SH-wave with $\phi_0 = 30°$. Frequency $k = 4$.

PHILOSOPHICAL TRANSACTIONS OF THE ROYAL SOCIETY A MATHEMATICAL, PHYSICAL & ENGINEERING SCIENCES

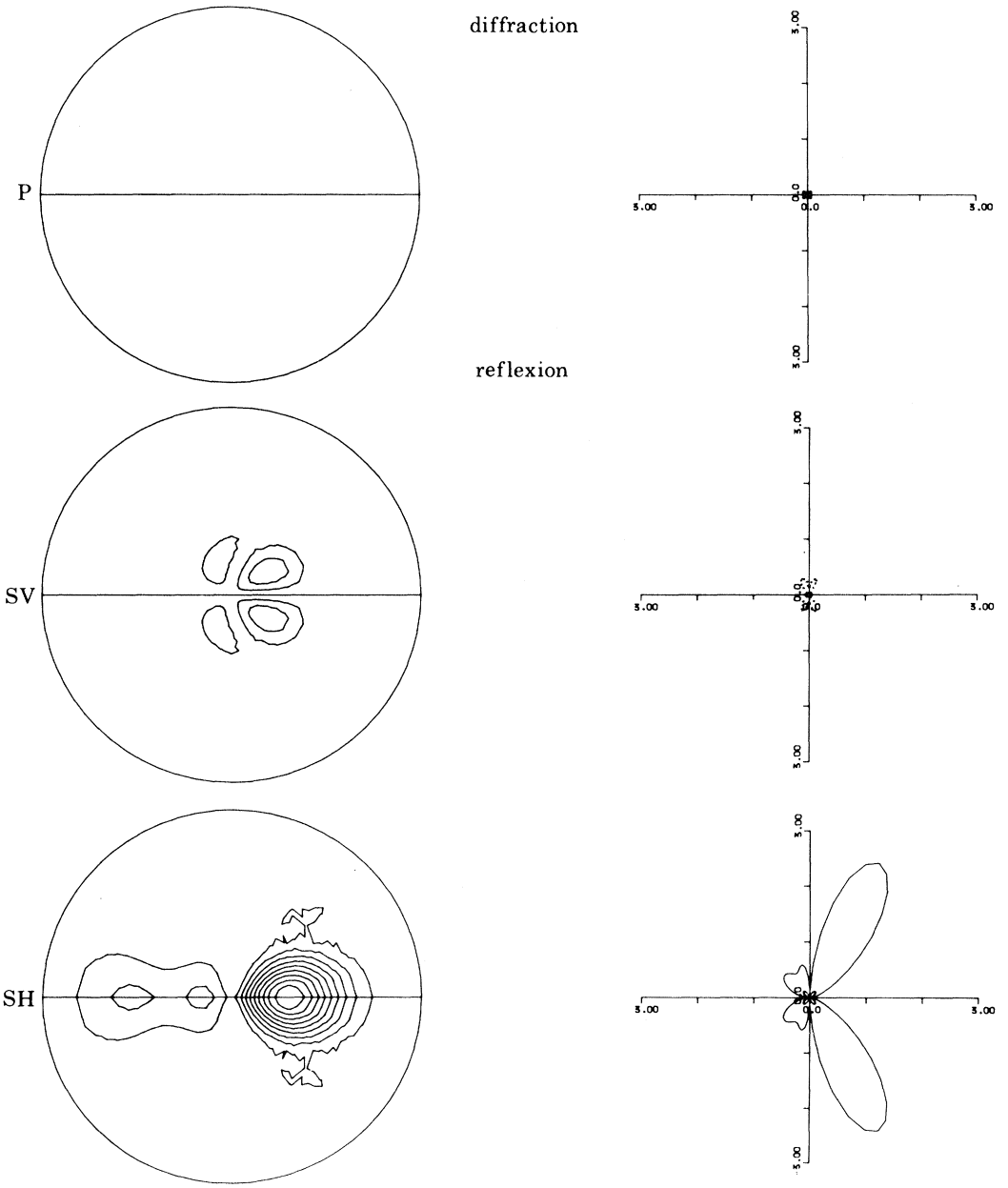

FIGURE 13. Amplitude contours and sections of scattered waves from incoming SH-wave with $\phi_0 = 20°$. Frequency $k = 8$.

PHILOSOPHICAL TRANSACTIONS OF THE ROYAL SOCIETY A MATHEMATICAL, PHYSICAL & ENGINEERING SCIENCES

References

Abramowitz, M. & Stegun, I. A. 1965 *Handbook of mathematical functions*. New York: Dover.

Achenbach, J. D. 1973 *Wave propagation in elastic solids*. Amsterdam: North Holland.

Barratt, P. J. & Collins, W. D. 1965 The scattering cross section of an obstacle in an elastic solid for plane harmonic waves. *Proc. Camb. phil. Soc.* **61**, 969–981.

Erdélyi, A. 1953 *Higher transcendental functions, vol.* 1. New York: McGraw-Hill.

Krenk, S. 1979 A circular crack under asymmetric loads and some related integral equations. *J. appl. Mech.* **46**, 821–826.

Krenk, S. 1981 Polynomial solutions to singular integral equations, with applications to elasticity theory. Dissertation, Risø National Laboratory.

Krenk, S. 1982 Some integral relations of Hankel transform type and applications to elasticity theory. *Integral equations and operator theory* **5**, 548–561.

Mal, A. K. 1968*a* Diffraction of elastic waves by a penny-shaped crack. *Q. appl. Math.* **26**, 231–238.

Mal, A. K. 1968*b* Dynamic stress intensity factor for an axisymmetric loading of the penny shaped crack. *Int. J. Engng Sci.* **6**, 623–629.

Mal, A. K. 1968*c* Dynamic stress intensity factor for a non-axisymmetric loading of the penny shaped crack. *Int. J. Engng Sci.* **6**, 725–733.

Mal, A. K. 1970 Interaction of elastic waves with a penny shaped crack. *Int. J. Engng Sci.* **8**, 381–388.

Martin, P. 1981 Diffraction of elastic waves by a penny-shaped crack. *Proc. R. Soc. Lond.* A **378**, 263–285.

Robertson, I. A. 1967 Diffraction of a plane longitudinal wave by a penny-shaped crack. *Proc. Camb. Phil. Soc.* **63**, 229–238.

Schmidt, H. & Krenk, S. 1982 Asymmetric vibrations of a cricular elastic plate on an elastic half space. *Int. J. Solids Struct.* **18**, 91–105.

Sezawa, K. 1929 Further studies on Rayleigh-waves having some azimuthal distribution. *Bull. Earthq. Res. Inst. Tokyo Univ.* **6**, 1–18.

Sih, G. C. & Loeber, J. F. 1968 Torsional vibration of an elastic solid containing a penny-shaped crack. *J. acoust. Soc. Am.* **44**, 1237–1245.

Sih, G. C. & Loeber, J. F. 1969 Normal compression and radial shear waves scattering at a penny-shaped crack in an elastic solid. *J. acount. Soc. Am.* **46**, 711–721.

Sneddon, I. N. 1972 *The use of integral transforms*. New York: McGraw-Hill.

Appendix A. Contour integration

The principle in the contour integration used here to reformulate the matrices A^m_{jl}, B^m_{jl} and C^m_{jl} is to write one of the spherical Bessel functions in the integrand as the sum of spherical Bessel functions of the third kind:

$$2j_n(s) = h^{(1)}_n(s) + h^{(2)}_n(s). \tag{A 1}$$

The argument is then extended to the complex half-plane $\mathrm{Re}\, z = s \geqslant 0$. For large values of z the asymptotic behaviour of the spherical Bessel functions of the third kind is (Abramowitz & Stegun 1965)

$$h^{(1,2)}_n(z) \sim \mathrm{i}^{\mp(n+1)} z^{-1} \mathrm{e}^{\pm \mathrm{i}z}, \quad |z| \gg 1. \tag{A 2}$$

The part of the integrand containing $h^{(1)}_n(z)$ therefore behaves asymptotically like $|z|^{-2}$ in the upper half-plane, while that containing $h^{(2)}_n(z)$ behaves asymptotically like $|z|^{-2}$ in the lower half-plane.

With the definitions (2.11) and (2.12) of $\alpha(s)$ and $\beta(s)$ the path of integration is $z = s + \mathrm{i}0$. The distinction between this path and $z = s - \mathrm{i}0$ is only necessary in the interval $0 < s < k$.

The matrix A^m_{jl} defined by (4.7) is used as an example. In anticipation of a special convergence problem the integral is expressed by the limit

$$A^m_{jl} = -\frac{4}{k^2} \lim_{\epsilon \to 0+} \int_\epsilon^\infty \left\{ \frac{(s^2 - \tfrac{1}{2}k^2)^2}{s\alpha(s)} - s\beta(s) \right\} j_{m+2j+1}(s) j_{m+2l+1}(s)\, \mathrm{d}s. \tag{A 3}$$

By use of (A 1)

$$A^m_{jl} = -\frac{2}{k^2} \lim_{\epsilon \to 0+} \int_\epsilon^\infty \left\{ \frac{(s^2 - \tfrac{1}{2}k^2)^2}{s\alpha(s)} - s\beta(s) \right\} \{ h^{(1)}_{m+2j+1}(s) + h^{(2)}_{m+2j+1}(s) \}\, j_{m+2l+1}(s)\, \mathrm{d}s. \tag{A 4}$$

For any finite value of ϵ the integral can be separated into two parts, one containing $h^{(1)}_{m+2j+1}(s)$ and another containing $h^{(2)}_{m+2j+1}(s)$.

The first term is now integrated along the closed contour in figure 14*a*, while the second is integrated along the contour in figure 14*b*. As neither of the integrands contains any poles within the contours, the original integrals in (A 4) can be replaced by integrals over the remainder of the contours, taken in the opposite direction. In these integrals the large quarter circles do not contribute. Furthermore, the contributions from the imaginary axis cancel as a consequence of the symmetry relation

$$h^{(1)}_{m+2j+1}(-z)\,j_{m+2l+1}(-z) = h^{(2)}_{m+2j+1}(z)\,j_{m+2l+1}(z). \tag{A 5}$$

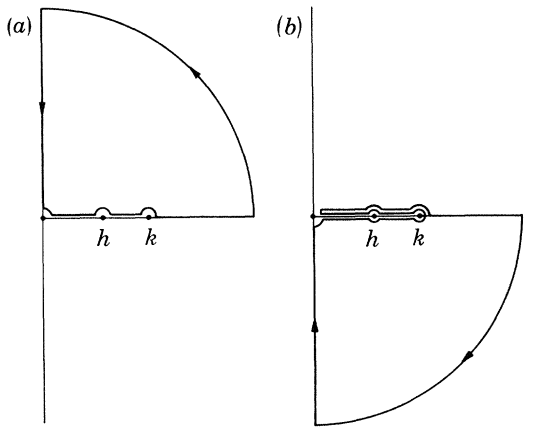

FIGURE 14. Integration contours in the complex s-plane: (*a*) $h^{(1)}_n$-contour; (*b*) $h^{(2)}_n$-contour.

The contributions from the small quarter circles depend on the asymptotic behaviour of the integrand as $z \to 0$. Thus the deciding factor is

$$h^{(1,2)}_{m+2j+1}(z)\,j_{m+2l+1}(z) \sim \mp \mathrm{i}\{(2m+4l+1)!!/(2m+4j+3)!!\}\,z^{2l-2j-1}.$$

As $A^m_{jl} = A^m_{lj}$ it is no restriction to impose the condition $j \leqslant l$, and it then follows from expansion of the full integrand in (A 4) that the small quarter circles only contribute to the diagonal terms A^m_{jj}:

$$A^m_{jl} = \lim_{\epsilon\to 0+}\left\{-\frac{4}{k^2}\int_\epsilon^h \frac{(s^2-\frac{1}{2}k^2)^2}{s\alpha(s)}\,h^{(2)}_{m+2j+1}(s)\,j_{m+2l+1}(s)\,\mathrm{d}s + \frac{4}{k_2}\int_\epsilon^k s\beta(s)\,h^{(2)}_{m+2j+1}(s)\,j_{m+2l+1}(s)\,\mathrm{d}s \right.$$
$$\left. + \frac{k^2}{2h}\frac{\delta_{jl}}{2m+4j+3}\left(\int_{z=\epsilon}^{z=\mathrm{i}\epsilon}\frac{\mathrm{d}z}{z^2} + \int_{z=\epsilon}^{z=-\mathrm{i}\epsilon}\frac{\mathrm{d}z}{z^2}\right)\right\}, \tag{A 7}$$

where δ_{jl} is the Kronecker delta. Evaluation of the last two integrals leads to the expression

$$A^m_{jl} = \lim_{\epsilon\to 0+}\left\{\frac{4\mathrm{i}}{k^2}\int_\epsilon^h \frac{(s^2-\frac{1}{2}k^2)^2}{s(h^2-s^2)^{\frac{1}{2}}}\,h^{(2)}_{m+2j+1}(s)\,j_{m+2l+1}(s)\,\mathrm{d}s \right.$$
$$\left. + \frac{4\mathrm{i}}{k^2}\int_\epsilon^k s(k^2-s^2)^{\frac{1}{2}}\,h^{(2)}_{m+2j+1}(s)\,j_{m+2l+1}(s)\,\mathrm{d}s + \frac{k^2}{\epsilon h}\frac{\delta_{jl}}{2m+4j+3}\right\}. \tag{A 8}$$

Although this expression contains in essence the desired reformulation of A^m_{jl}, it is inconvenient for numerical integration. The final step is therefore to express the last factor as an integral over the interval $[\epsilon, h]$, and it is desirable that this integral should be a product of a smooth function and the weight function $(h^2-s^2)^{-\frac{1}{2}}$. The optimal choice appears to be the integral

$$\int_\epsilon^h \frac{\mathrm{d}s}{s^2(h^2-s^2)^{\frac{1}{2}}} = \frac{(h^2-\epsilon^2)^{\frac{1}{2}}}{h^2\epsilon} = \frac{1}{h\epsilon} + O(\epsilon). \tag{A 9}$$

When this relation is used to eliminate the factor ϵ^{-1} from (A 8), each integral becomes continuous in the limit $\epsilon = 0$, and the result is

$$A_{jl}^{m} = \int_0^h \left\{ \frac{4\mathrm{i}}{k^2} \frac{(s^2 - \frac{1}{2}k^2)^2}{s(h^2 - s^2)^{\frac{1}{2}}} h_{m+2j+1}^{(2)}(s) j_{m+2l+1}(s) + \frac{k^2}{2m+4j+3} \frac{\delta_{jl}}{s^2(h^2 - s^2)^{\frac{1}{2}}} \right\} \mathrm{d}s$$
$$+ \int_0^k \frac{4\mathrm{i}}{k^2} s(k^2 - s^2)^{\frac{1}{2}} h_{m+2j+1}^{(2)}(s) j_{m+2l+1}(s)\, \mathrm{d}s. \quad \text{(A 10)}$$

Appendix B. Two exponental integrals

The asymptotic form of the displacements requires evaluation of integrals of the form

$$I_1 = \lim_{r\to\infty} r^{\frac{1}{2}} \int_0^{\frac{1}{2}\pi} F(\psi)\, \mathrm{e}^{\mathrm{i}2r\cos^2\frac{1}{2}(\psi+\phi)}\, \mathrm{d}\psi, \quad \text{(B 1)}$$

$$I_2 = \lim_{r\to\infty} r^{\frac{1}{2}} \int_0^{\frac{1}{2}\pi} G(\psi)\, \mathrm{e}^{\mathrm{i}2r\sin^2\frac{1}{2}(\psi-\phi)}\, \mathrm{d}\psi, \quad \text{(B 2)}$$

where $F(\psi)$ and $G(\psi)$ are differentiable in the closed interval $[0, \frac{1}{2}\pi]$, and $0 < \phi < \frac{1}{2}\pi$.

The integral I_1 is evaluated by observing that $\tau = \cos^2\frac{1}{2}(\psi+\phi)$ is a monotonic function of ψ and therefore a suitable integration variable:

$$I_1 = \lim_{r\to\infty} r^{\frac{1}{2}} \int_{\cos^2\frac{1}{2}(\phi+\frac{1}{2}\pi)}^{\cos^2\frac{1}{2}\phi} \frac{F(\tau)}{\tau(1-\tau^2)^{\frac{1}{2}}}\, \mathrm{e}^{\mathrm{i}2r\tau}\, \mathrm{d}\tau. \quad \text{(B 3)}$$

It now follows from the Riemann–Lebesgue lemma (for example in the form given by Sneddon (1972, p. 30)) that $I_1 = 0$ for $0 < \phi < \frac{1}{2}\pi$.

The integral I_2 is evaluated by use of the following result, known from the limit at infinity of the Fresnel integrals (Abramowitz & Stegun 1965):

$$\lim_{r\to\infty} r^{\frac{1}{2}} \int_0^{\frac{1}{2}\pi} \cos\tfrac{1}{2}(\psi-\phi)\, \mathrm{e}^{\mathrm{i}2r\sin^2\frac{1}{2}(\psi-\phi)}\, \mathrm{d}\psi$$
$$= \lim_{r\to\infty} 2^{\frac{1}{2}} \int_{(2r)^{\frac{1}{2}}\sin\frac{1}{2}\phi}^{(2r)^{\frac{1}{2}}\sin\frac{1}{2}(\frac{1}{2}\pi-\phi)} \mathrm{e}^{\mathrm{i}r^2}\, \mathrm{d}\tau = 2^{\frac{3}{2}} \int_0^{\infty} \mathrm{e}^{\mathrm{i}\tau^2}\, \mathrm{d}\tau = (2\pi)^{\frac{1}{2}}\, \mathrm{e}^{\frac{1}{4}\mathrm{i}\pi}. \quad \text{(B 4)}$$

By addition and subtraction

$$I_2 = (2\pi)^{\frac{1}{2}}\, \mathrm{e}^{\frac{1}{4}\mathrm{i}\pi} G(\phi) + \lim_{r\to\infty} r^{\frac{1}{2}} \int_0^{\frac{1}{2}\pi} \{G(\psi) - G(\phi)\cos\tfrac{1}{2}(\psi-\phi)\}\, \mathrm{e}^{\mathrm{i}2r\sin^2(\psi-\phi)}\, \mathrm{d}\psi. \quad \text{(B 5)}$$

Again the Riemann–Lebesgue lemma may be used to prove that the limit of the integral in (B 5) is zero, leaving

$$I_2 = (2\pi)^{\frac{1}{2}}\, \mathrm{e}^{\frac{1}{4}\mathrm{i}\pi} G(\phi). \quad \text{(B 6)}$$